Molecular dynamics study on water and hydroxide transfer mechanisms in PSU-g-alkyl-TMA membranes at low hydration: Effect of side chain length

Pierre Magnico

Author's remarks

Two corrections have been made in the uncorrected proof:

1/ In the main text:
Huo et al. [82] must be corrected as Huo et al. [79].

2/ In the refecrence section:

Ref. [26] must be read as:

Takaba H., Hisabe T., Shimizu T., Alam Md. K. Molecular modeling of OH- transport in poly(arylene ether sulfone ketone)s containing quaternized ammonio-substituted fluorenyl groups as anion exchange membranes. J Membr Sci 2017;522:237–244.

INTERNATIONAL JOURNAL OF HYDROGEN ENERGY XXX (XXXX) XXX

Available online at www.sciencedirect.com

ScienceDirect

journal homepage: www.elsevier.com/locate/he

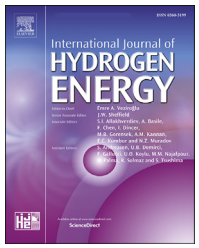

Molecular dynamics study on water and hydroxide transfer mechanisms in PSU-g-alkyl-TMA membranes at low hydration: Effect of side chain length

Pierre Magnico

Lab. M2P2, Ecole Central Marseille, 38 Rue Joliot-Curie, 13451, Marseille, France

HIGHLIGHTS

- Molecular dynamics is carried out with alkylammonium-g-PSU based membranes.
- The influence of the spacer length, the water uptake, the temperature on the anion and water transfer is studied.
- The residence time around the functional sites decreases with these three parameters.
- "Hopping" and "caging" motions are observed with the self-part of the Van Hove functions.
- The hydrogen bond network depends on the spacer length at very small water content.

ARTICLE INFO

Article history:
Received 27 April 2021
Received in revised form
1 July 2021
Accepted 13 July 2021
Available online xxx

Keywords:
Anion exchange membrane
Molecular simulation
Hydroxide ion
Cluster
Vehicular diffusion

ABSTRACT

Molecular dynamics simulations with anion exchange membranes (alkyl trimethyl ammonium grafted onto polysulfone) are performed to investigate the influence of the spacer length on the transport properties, on the molecular exchange mechanisms between the functional group and the aqueous phase and on the hydrogen bond network. This is especially insightful that in this work the hydration number is small. In this condition the aqueous phase must be thought as an assembly of small clusters. The results show an unexpected dependence of the water and hydroxide (OH) diffusivity on the temperature and the water uptake. The distribution of the cluster size bonded to OH explain partially the OH diffusivity. "Hopping" and "caging" motions are observed with the self-part of the Van Hove functions even at high temperature. The characteristic time of the survival probability correlation function around the functional groups is a decreasing function of the alkyl length.

Introduction

Ion exchange membranes (IEM) play an important role for a wide range of engineering applications [1] such as separation processes (electrodialysis, diffusion dialysis, capacitive deionization) and energy production and conversion (reverse electrodialysis, fuel cells and redox flow batteries) [2–4]. The IEM are divided in two groups, depending on the charge of the functional groups grafted onto the polymeric backbone: the proton (PEM) and the anion exchange membranes (AEM) [5,6].

E-mail address: pierre.magnico@univ-amu.fr.

https://doi.org/10.1016/j.ijhydene.2021.07.081

Please cite this article as: Magnico P, Molecular dynamics study on water and hydroxide transfer mechanisms in PSU-g-alkyl-TMA membranes at low hydration: Effect of side chain length, International Journal of Hydrogen Energy, https://doi.org/10.1016/j.ijhydene.2021.07.081

Regarding the fuel cell (FC) technology, the PEMFC (proton exchange membranes for fuel cell) present several drawbacks despite their high performance and their long lifetime. PEMFC require platinum (pt) or precious metal-based catalysis and cell hardware resistance to the corrosion. It is only recently that AEMFC (anion exchange membranes for fuel cell) are regarded as a promising alternative [7–10]. In these systems, the hydroxide anions (OH) are generated by the oxygen reduction at the cathode and transfer the electric charge. Therefore, the AEMFC present several advantages such as the use of Ni-based catalysis and the alkalinity of these fuel cells [11–13]. However, the main issue is the chemical stability of the polymer because the OH is a strong nucleophile. This induces the use of an operating condition with high water content and a temperature lower than 60 °C [14–21].

At high water content, the hydrophobic phase, formed by the polymeric backbone, is well separated from the hydrophilic phase formed by the percolating water channel. The functional groups are located between the two phases [22–24]. The hydrogen bond (HB) connectivity is high enough for the aqueous phase to be homogeneous and continuous. Owing to the close water coordination network around the OH ion (i.e the hyperconnectivity), the anion diffusion is highly dependent on the solvation structure [25], but also of the electrostatic interaction with the cationic groups. In bulk aqueous solution, it is admitted that the anion diffusion is controlled by two mechanisms: the Grotthus mechanism (or structural diffusion) in which transfer of the charge defect is provided by successive formation/breakings HB between surrounding water molecules, and the vehicular mechanism in which formation/breakings HB reactions are not involved in the charge transfer. In hydrated membranes, the analysis with ab initio molecular dynamics (AIMD) and classical MD, the two mechanisms occur, the structural diffusion being the main process [26,27].

At low water content, the aqueous phase can no more be regarded as a continuous phase. The HB network must be described as a set of clusters which size distribution depends on the water content. As it decreases, the size of the water channel and the hydration of the functional groups decreases. At the same time, the water coordination around the oxygen of the hydroxide ion (Oh) decreases also. This leads to the increase of the vehicular process contribution on the hydroxide mobility. In the case of quaternary ammonium (QA), the threshold of the hydration level λ_N (No of water molecules per function group), over which the AEM is hydrated enough to contain continuous channel, is unknown. However, in the case of Nafion 117, the structural diffusion is dominant if $\lambda_N > 10$ [28]. AIMD simulations on idealized structures functionalized with QA groups and on QSEBS (styrene-ethylene-butylene-styrene) show that below a threshold value of 6 the anion mobility is controlled by the vehicular mechanism [29–31]. MD simulations with BTEA (benzyltriethyl ammonium) how that water bridged hydroxide pairs characterizes the aqueous structure. When $\lambda_N > 4$, a hydrogen-bonded network forms and the concentration of these pairs decreases with the increasing λ_N [32,33].

A way to enhance the segregation between the hydrophilic and the hydrophobic phase and to enhance the alkaline stability consists in increasing the anionic graft length. This allows to take away the hydroxide ions from the backbone. The hydrophobicity of the long chain tends to form more efficient hydrophilic phase topology and to increase the anionic conductivity and/or chemical stability of the ammonium group [8,17,19,34–42]. In the case of the QA group, the graft (also named side chain) can be tuned by increasing the length of the intermediate alkyl chain (spacer unit) or by substituting one of the methyl group for a longer chain (extender chain) [17,18,37,39,43,45]. Coarse grained MD with a PPO (polyphenylene oxide) backbone show that hydrophilic morphology can be designed by the pattern of the tethering from the lamellar structure to a more interconnected one [46,47]. Adding several cationic groups in the same side chain or tuning the hydrophobicity of the side chain are another way to increase the variety of the aqueous morphology [48–51].

In the present work, the classical MD are carried out to investigate the possible impact of the spacer length with an alkyl-trimethyl ammonium grafted onto a PSU backbone in the case of a small hydration level of 3 and 6. However, the length of the spacer is much smaller than the length used in the studies mentioned above. In order to compare the transport properties of the hydroxide ion, of the water molecule and of the QA group, four alkyl chains are used, from the methyl to the butyl chain. The diffusion process is not only influenced by the aqueous phase morphology but depends on the interaction with the functional group and on the hydration shells around the anions and the water molecules. To explore these aspects, the residence time distribution around the QA group and the distinct Van Hove functions (QA/OH) and (QA/H_2O) are examined first. Then the self Van Hove functions of H_2O and of OH are analyzed and finally, the hydrogen bond network is described. As the classical MD is performed, the structural diffusion is not taken into account.

Model construction and methodology

The goal of the present work is to analyze the influence of the spacer length on the transfer mechanism of water molecules (H_2O) and of hydroxide ions (OH) at the local scale and at the model scale. As a first step, a polymer containing 10 monomers is built with the software AMBER [52]. Each monomer (PSU) is functionalized with an ammonium group grafted by means of an intermediate alkyl chain which contains one to four carbon atoms (see Fig. 1). In a 2nd step, four polymers with 40 hydroxide ions and a variable number of water molecules depending on the water uptake (WU) are inserted in a simulation box with a side length of 100 Å by means of the software PACKMOL [53,54]. As a 3rd step several annealing cycles are performed in order to reach a relaxed configuration. The characteristics of the eight membrane systems are gathered in Table 1.

A first annealing cycle consists in a heating at T = 600 K, a cooling at T = 300 K in the NVT ensemble (N: No of atoms, V:

Please cite this article as: Magnico P, Molecular dynamics study on water and hydroxide transfer mechanisms in PSU-g-alkyl-TMA membranes at low hydration: Effect of side chain length, International Journal of Hydrogen Energy, https://doi.org/10.1016/j.ijhydene.2021.07.081

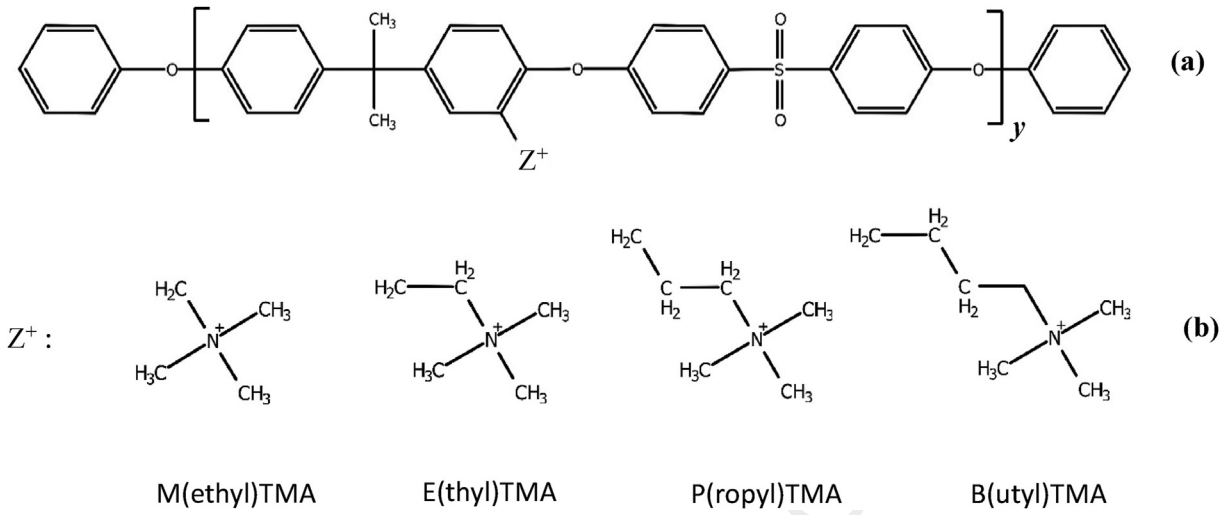

Fig. 1 – Chemical structures of model polymers. (a) PSU; (b): graft (Z^+) composed of a carbon chain (Methyl, Ethyl, Propyl, Buthyl) bonded to an ammonium group (trimethyl ammonium).

Table 1 – Summary of the amorphous membranes. Crosses mean that the MD is not performed.

	MTMA		ETMA		PTMA		BTMA	
Molecular weight	5149		5289		5429		5570	
Water uptake (wt%)	10	20	10	20	10	20	10	20
Hydration level (λ_N)	2.86	5.72	2.94	5.88	3.02	6.03	3.09	6.19
No of OH-	40	40	40	40	40	40	40	40
No of H2O	114	229	118	235	121	241	124	248
Cell size (Å) 300 K	31.58	32.34	31.88	32.7	32.25	33.16	32.64	33.56
Density (g/cm^3) 300 K	1.23	1.25	1.23	1.21	1.22	1.22	1.2	1.2
Cell size (Å) 353 K	31.69	32.53	X	X	X	X	32.81	33.63
Density (g/cm^3) 353 K	1.22	1.23	X	X	X	X	1.18	1.2

volume, T: Temperature) and a final molecular dynamics (MD) computation in NPT ensemble performed during 500 ps in order to obtain a first dense membrane with an imposed pressure (P) of 1bar. Then several cycles of heating (NVT) at 600 K, cooling back at 300 K (NVT) and relax step (NPT) at 1bar and 300 K are performed over a period of 100 ps, 60 ps and 60 ps respectively until a constant density is reached. Fig. SI-01 shows the density in function of the carbon number of the spacer (N_C), WU and T. As a last step, before the data acquisition, a MD simulation is performed during 1 ns in NPT ensemble with a pressure of 1bar and a temperature of 300 K or 353 K.

The MD simulations are carried out with DLPOLY package [55]. The AMBER force field GAFF2 [56] and the periodic boundary condition in the three directions are input by means of the software DL_FIELD [57]. The OH are modeled with the parameters of Jang et al. [58] and the TIP4P-2005 water model is used [59]. The partial charge of the functionalized polymer is computed through the Mulliken population analysis using B3LYP and 6-31G**. The equation of motion is integrated using the velocity Verlet algorithm combined with the Nosé-Hoover thermostat and barostat with a time step of 1 fs. The relaxation times are 0.5 ps. The electrostatic interactions are computed by considering the Ewald sum. The truncation length of all the interactions is set at 11.5 Å. Fig. 2 displays two examples of simulated membranes.

Results and discussion

Radial distribution function

We first describe the molecular system by means of the radial distribution function (RDF) g(r) and the coordination number CN. The CN of atom B around an atom A inside a shell of radius R_A is defined as:

$$CN_{A-B} = 4\pi \frac{N_A}{V} \int_0^{R_A} r^2 g_{A-B}(r) dr \quad (1)$$

where N_A is the total number of atom A, V is the volume of the system and $g_{A\text{-}B}(r)$ is the radial distribution function of A around B. Its expression is:

$$g_{A-B}(r) = \left(\frac{n_B}{4\pi r^2 dr}\right) \Big/ \left(\frac{N_B}{V}\right) \quad (2)$$

where n_B is the number of atom B located in a shell of thickness dr at a distance r from atom A. N_B is the total number of atom B.

Fig. 3 compares the N–N, N-Oh and N-Ow RDF between the MTMA membrane ($N_C = 1$) and the BTMA one ($N_C = 4$) for the two WU. Oh and Ow mean the oxygen atom of OH and H_2O respectively. From now, N means the nitrogen atom of the

Please cite this article as: Magnico P, Molecular dynamics study on water and hydroxide transfer mechanisms in PSU-g-alkyl-TMA membranes at low hydration: Effect of side chain length, International Journal of Hydrogen Energy, https://doi.org/10.1016/j.ijhydene.2021.07.081

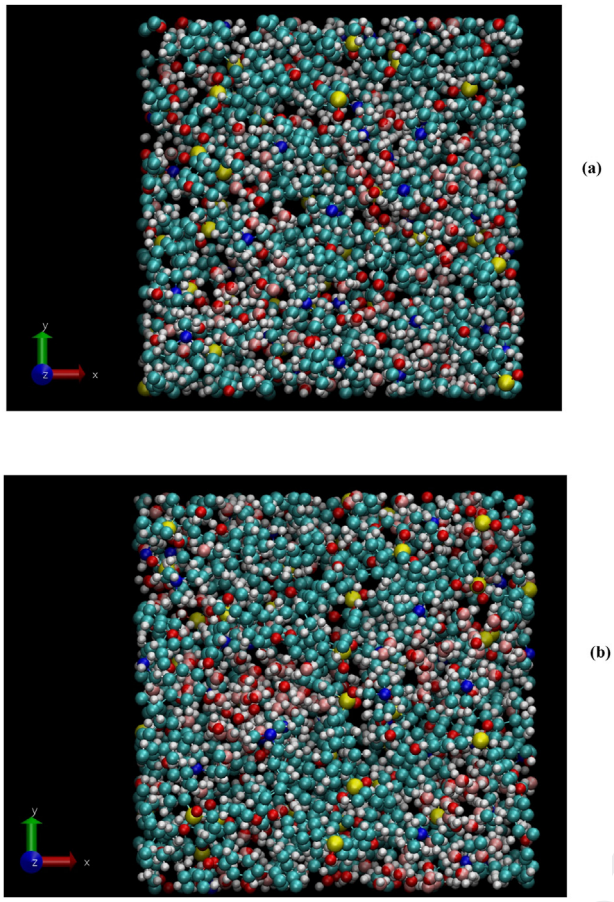

Fig. 2 – Two snapshots of a simulation box of PSU-g-BTMA for two hydration levels at T = 300 K. (a): WU = 10%; (b): WU = 20%. The box size is 33 Å. Color chart: Light blue (carbon), dark blue (nitrogen), yellow (sulfur), white (hydrogen), red (oxygen), pink (ghost atom of the TIP4P water molecule). (For interpretation of the references to color in this figure legend, the reader is referred to the Web version of this article.)

ammonium group. Tables SI-01 and 02 gather the peak positions and the coordination numbers CN of all the samples used in the present work. The coordination numbers are computed over the first shell volume which radius is equal to the radiale position of the first minimum. Its value is in parenthesis in Tables SI-01(b) and SI-02(b).

The Figures show the agreement with the profiles published in Refs. [58,60,61]. Owing to the length of the grafts, the published results must be compared with the BTMA ones. We must keep in mind that the articulation and the volume of the spacer and of the backbone depend on their constituents. The system used in Ref. [58] is close to the present one as concerns WU and the backbone even if three ammonium groups are grafted onto two monomers. In the two other publications [60,61], the radial profiles of the RDF and of the CN are reported for $\lambda_N = 14$ and the backbone is a polyvinyl in which one methyl out of two is functionalized. Fig. 3 and Tables SI-01 and 02 show that the position of the peaks is smaller than in the publications by 0.5 Å to 1 Å and that the main peak of N-Ow and N-Oh RDF is composed of a doublet which is also observable in Ref. [62]. The N–N CN (Tables SI–01(b)) varies from 1 to 1.9 and from 0.5 to 1 for WU = 10% and 20% respectively at T = 300 K. If T = 353 K (Tables SI–02(b)), the value of N–N CN is 1.45 and 1 as WU increases. In Refs. [60,61], its value is 1.4 and a little greater than 2 respectively. The N-Ow CN is close to the value found in Ref. [58] (7 and 11.5 for WU = 10% and 20% respectively). The N-Oh CN agrees the value observed in Refs. [60,61] (2. and 2.2 respectively). The peak height of the three RDF decreases with WU. This is related to the fact that 1) the N–N CN decreases with WU as the hydration moves away the ammonium groups [58], 2) the N-Ow CN increases by a factor lower than 2 with WU and 3) the N-Oh CN is independent of WU.

As concerns the aqueous phase, Figs. (SI_02), the peak positions are the same as in the three publications. However, in the case of Ow-Ow RDF with WU = 10%, a shoulder is located at r = 3 Å. Shoulders are also observable in Ow-Ow and N-Ow RDF profiles but with a much smaller amplitude in Ref. [58]. The Oh-Ow CN at 353 K agrees the values observed in Ref. [58]. Its value varies from 3.6 to 4.1 and from 5 to 5.3 for WU = 10% and 20% respectively at T = 300 K which is close to the value of 4 observed in Refs. [60,61]. The peak height of the Oh-Ow RDF is a decreasing function of WU because the CN increase rate is lower than the WU one. The Ow-Ow CN increases with WU revealing an increasing number of hydrogen bond between water molecules, i.e an increase of the cluster size, as we will see below.

Diffusion coefficient

It must be reminded that we take into account of the vehicular diffusion process only. Fig. 4 show the self-diffusion coefficient vs. the carbon number of the spacer. The self-diffusion coefficient is computed in the linear part of the MSD by the following equation:

$$D = \lim_{t\to\infty} \frac{1}{6t} \langle (r(t) - r(0))^2 \rangle \quad (3)$$

where $r(t)$ and $r(0)$ are the radial position of Ow, of Oh and of N at time t and 0 respectively. In Fig. 4(b), the computed values of D_{Ow} (T = 353 K) with Eq. (3) are divided by 4 to make the figure easier to read. Fig. SI-03 present typical mean square displacements (MSD) of Ow, Oh and N. The straight line related to D_N in Fig. SI-03(b) is shifted to smaller values in order to show that the MSD follow the same increase rate in the time range [45,80] ns.

In the case WU = 10% (Fig. 4(a)), the three diffusion coefficients present a convex profile with a minimum for $N_C = 3$ (PTMA). Surprisingly, the intuitive hierarchy $D_{Ow} > D_{Oh} > D_N$ is not always observed even if the curves have the same shape. The simulations give $D_{Oh} > D_{Ow}$ with MTMA for the two temperatures. We can also observe the inequality $D_N > D_{Ow} > D_{Oh}$ with BMTA and the little effect of temperature on D_{Oh} and D_{Ow} (MTMA). For the two other polymers EMTA and PMTA, $D_{Oh} \sim D_{Ow}$. On contrary with the condition WU = 20%, the inequality $D_{Ow} > D_{Oh} > D_N$ is observed whatever the value of N_C. If T = 300 K, D_{Ow} increases with N_C and D_{Oh} is almost constant. At this temperature, the profile of D_N seems to be erratic. It is not correlated to the N–N CN. This behavior does not affect the diffusivity of H_2O and OH. Finally, D_{Oh} and D_{Ow}

Please cite this article as: Magnico P, Molecular dynamics study on water and hydroxide transfer mechanisms in PSU-g-alkyl-TMA membranes at low hydration: Effect of side chain length, International Journal of Hydrogen Energy, https://doi.org/10.1016/j.ijhydene.2021.07.081

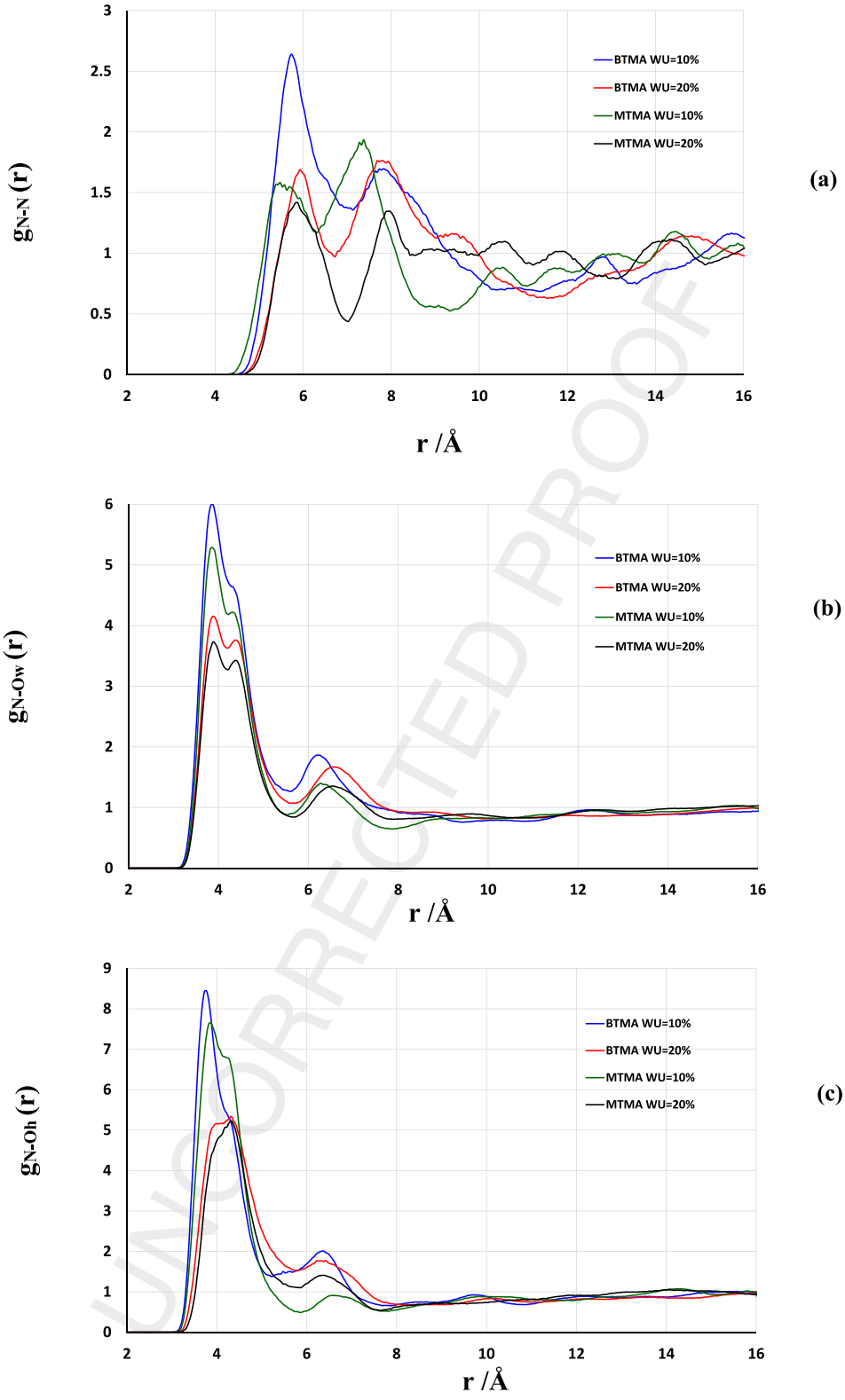

Fig. 3 – Radial correlation function for different membranes and water uptakes. T = 300 K. (a): g_{N-N}; (b): g_{N-Ow}; (c): g_{N-Oh}.

are much more sensitive to the temperature than with the condition WU = 10%.

The figures also show that at T = 300 K, D_{Ow} and D_{Oh} increase with WU except for MTMA and for BTMA as concerns D_{Oh} (decrease of 15%). The decrease of D_{Ow} and D_{Oh} with WU is not observed at T = 353 K. It is admitted that the diffusion coefficient increases with WU. However, the small decrease of D_{Oh} (BTMA at 300 K) cannot be regarded as a real one. Its amplitude is smaller than the computation accuracy and statistical fluctuations must be taken into account (see for

Please cite this article as: Magnico P, Molecular dynamics study on water and hydroxide transfer mechanisms in PSU-g-alkyl-TMA membranes at low hydration: Effect of side chain length, International Journal of Hydrogen Energy, https://doi.org/10.1016/j.ijhydene.2021.07.081

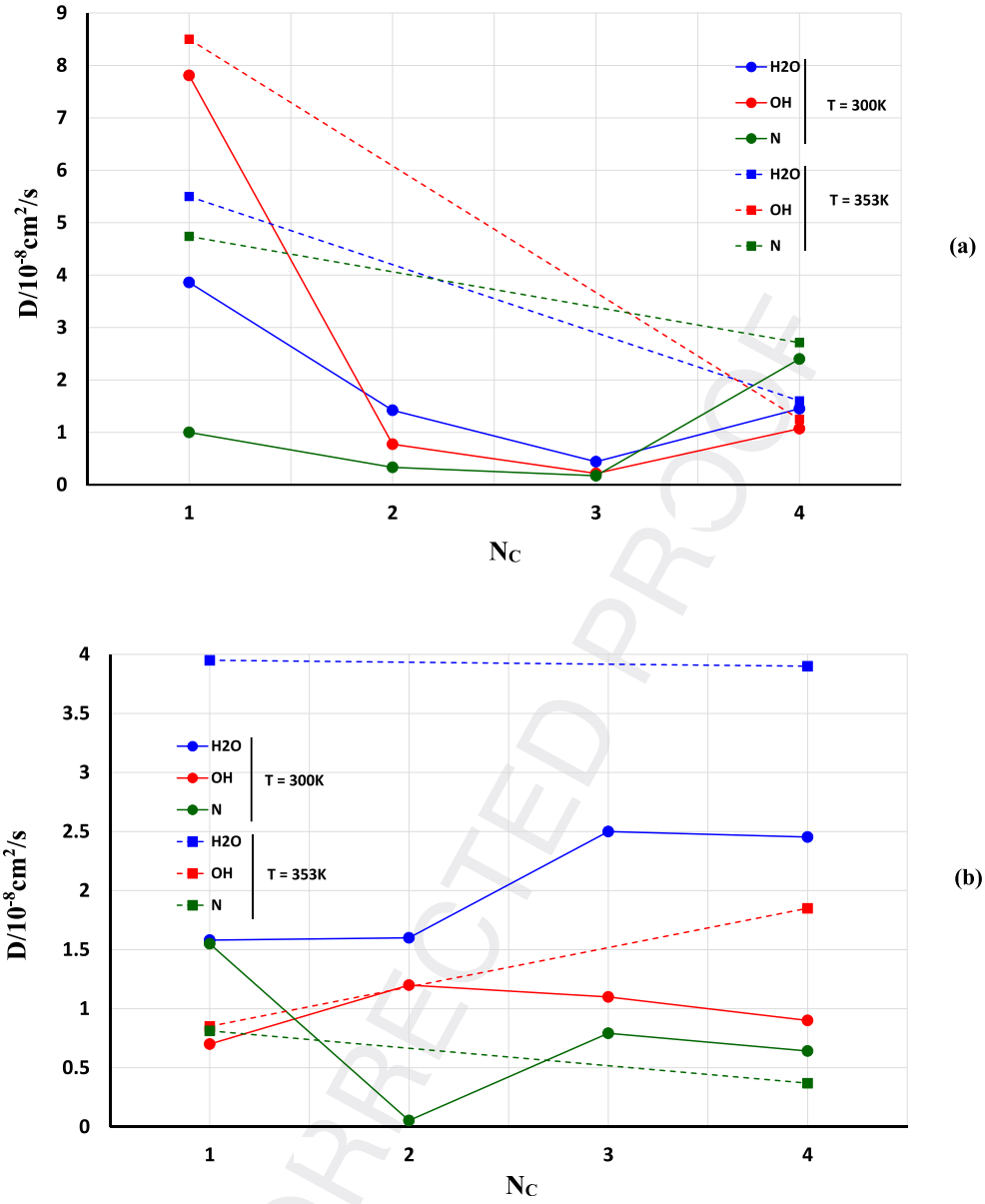

Fig. 4 – Diffusion coefficient of Ow, Oh and N vs. number of carbon atom in the alkyl chain. (a) WU = 10%; (b) WU = 20%. The two values of D_{Ow} (T = 353 K-WU = 20%) in figure (b) are divided by 4.

instance Fig. 2 in Ref. [33] and Fig. 3 in Ref. [62]). As concerns MTMA, the RDF do not reveal any anomalies, nor in the membrane structure nor in the aqueous phase repartition around the ammonium groups, which could explain this surprising result. Moreover, this is confirmed by the analysis of the spatial distribution of the functional groups which displays a homogeneous distribution (not shown in the manuscript) and by the invariance of D_N with WU.

Han et al. [58] computed at T = 353 K a value of 5.7×10^{-8} cm^2/s (WU = 10%) and 7.38×10^{-7} cm^2/s (WU = 20%) for D_{Ow} and a value of 1.6×10^{-9} cm^2/s (WU = 10%) and 3.7×10^{-8} cm^2/s (WU = 20%) for D_{Oh}. In the case of BTMA the same order of magnitude is obtained but lower. The value of D_{Ow} is 1.6×10^{-8} cm^2/s (WU = 10%) and 1.5×10^{-7} cm^2/s (WU = 20%) and D_{Oh} is 1.3×10^{-8} cm^2/s (WU = 10%) and 1.8×10^{-8} cm^2/s (WU = 20%). The discrepancy concerns D_{Oh} with WU = 10%.

Generally, experimental investigation with AEMFC show that the conductivity increases by a factor of 2–4 if T increases from 300 K to 353 K [18,20,21,38,40–42,44,45,50,51]. The expression of the Arrhenius law gives an activation energy (E_A) ranging from 12 to 23 kJ/mol. However, we keep in mind that water content and swelling tend to increase with the temperature. This may induce an increase of E_A. In the present work D_{Oh} (WU = 20%) increases by a factor of 1.2 (E_A = 3.5 kJ/mol) and of 2 (E_A = 12 kJ/mol) for MTMA and BTMA respectively. If WU = 10%, D_{Oh} is quite invariant with T for these two membranes. In Ref. [60] MD computations give a factor value of 13 (E_A = 42 kJ/mol) for λ_N = 14 with the non-scaled data. With the same membrane as in Ref. [60], Chen et al. [61]

Please cite this article as: Magnico P, Molecular dynamics study on water and hydroxide transfer mechanisms in PSU-g-alkyl-TMA membranes at low hydration: Effect of side chain length, International Journal of Hydrogen Energy, https://doi.org/10.1016/j.ijhydene.2021.07.081

computed a factor of 3.5 (E_A = 21 kJ/mol) with AIMD (NVT ensemble and MSD over 1 ns).

As concerns the diffusivity of water in the present work, D_{Ow} (WU = 20%) increases by a factor of 6.5 (E_A = 31 kJ/mol) and of 10 (E_A = 38 kJ/mol) for BTMA and MTMA respectively. This factor is 8.2 (E_A = 35 kJ/mol) and 3 (E_A = 18 kJ/mol) in Ref. [60] (non-scaled data) and in Ref. [61] respectively. Experimental measurements of D_{Ow} by PGSE-NMR (pulse gradient spin echo-nuclear magnetic resonance) on two Poly (2,6 dimethyl 1,4 phenylene oxide)-b-Poly (vinyl benzyl trimethyl ammonium) membranes [63] give a value of 20 kJ/mol (λ_N = 14) and of 25 kJ/mol (λ_N = 10). These values are close to the ones computed in Ref. [61]. However, NMR investigations with Nafion [64–66] clearly show that E_A is a decreasing function of λ_N. At high water content ($\lambda_N > 10$) the value of E_A is equal to the value of pure water (i.e 20 kJ/mol). As λ_N decreases from 6 to 3 E_A increases from 25 ± 5 kJ/mol to 32.5 ± 4.5 kJ/mol. The results published in Ref. [63] seem to confirm this observation. So, E_A is certainly much greater than 20 kJ/mol at small water content in AEMFC and additional MD computations and experiments are needed owing to the high dispersion of published values.

Residence time

Intuitively, the self-diffusion process is thought to be the results of two kinds of interaction 1/between the aqueous phase and the functional groups and 2/between the hydroxide ions and the water molecules. But we will see that it is not as simple. The residence time spent close to the ammonium groups by the water molecules and the hydroxide ions is a way to examine the interaction between the aqueous phase and the polymer. This time is evaluated by means of the autocorrelation function C_R of the survival probability function P_{ij} (t_0, t_0+t) which takes the value of one if the molecule j is inside the first shell of the ammonium group i from time t_0 to time t_0+t, and zero otherwise [67,68]. The residence or correlation time is computed from the following equation:

$$\tau_R = \int_0^\infty C_R(t)dt \quad \text{with } C_R(t) = \sum_{i=1}^{N_{QA}} \sum_{j=1}^{N_{H20}} \frac{1}{N+m-1} \sum_{t_0} P_{ij}(t_0, t_0+t) \tag{4}$$

in which N is the total number time steps (δt) of simulation, m is the index defined by t = m δt, N_{QA}, is the total number of quaternary ammonium, N_{H2O} is the total number of water molecules.

The double exponential fit is often used in order to determine a short and a long-time scale [69,70]. The Kohlrausch-Williams-Watts equation $Aexp(-(t/\tau_R)^{\beta})$ can also be used to compute τ_R [60,69,71]. β is the stretching parameter which value is one in the case of an exponential phenomenon in the bulk and decreases to 0.5 or lower in the case of a residence time in a first shell. In order to determine the short and long-time scale two stretched exponentials are used. Dubey et al. [60] find a value of 0.3 and of 10.3 ps for β and τ_R respectively. However, the authors find a mean residence time of 232 ps (λ_N = 14) if the partial charges are not scaled. In the present work, C_R can be fitted with the KWW equation but not with the double exponential one. The exponential behavior is observed at long time which gives a much higher value of τ_R. Owing to the high difference of value between the characteristic times depending on the computation method, it is decided to use the simplest computation.

Fig. 5 and Table SI_03 and 04 display the variation of τ_R in function of N_C. The mean residence time is a decreasing function of N_C. When τ_R is greater than 10 ns, the C_R curve show an important contribution of the residence time greater than 50 ns. This means that some water molecules and hydroxide ions remain in the vicinity of an ammonium group until 100 ns and that the real value of τ_R is higher that the computed one. This is the reason why a sudden high value of τ_R is observed for ETMA (WU = 20%) with the hydroxide ion. However, this jump seems to have no consequence on the Oh diffusivity. As expected, τ_R is a decreasing function of T and WU and $\tau_R^{Oh} > \tau_R^{Ow}$. An unexpected behavior can be deduced from Figs. 4 and 5: τ_R^{Oh} and τ_R^{Ow} have the higher value for MTMA (WU = 10%, T = 300 K), but in this system and condition, D_{Oh} and D_{Ow} reach their highest value compared to the other polymers. In fact, the mean residence time does not mean that a molecule leaves a functional group definitively. $C_R(t)$ is a time distribution only. A molecule can go back or enter another ammonium shell after few time steps (1 fs). So, a molecule can be inside a shell for a time much greater than τ_R. The correlation between τ_R and D is not obvious even if τ_R is a decreasing function of T and D an increasing one. The N-Oh CN is around 2 whatever the system at 300 K and 353 K. So, as mentioned in Ref. [61], each hydroxide ion is in the first shell of 2 ammonium groups in average. This means that a OH ion can move through the simulation box without leaving the hydration shell during the MD simulation even for high water contents. This observation can be also applied to H_2O.

The use of τ_R assumes that we consider one shell at least. In other word, the value τ_R depends on the number of shells in which a molecule stays at the same time. We define τ_{Ri} as the time during which a molecule is inside i ammonium shells simultaneously. In Tables SI-03 and 04 are gathered the τ_{Ri} of Ow and Oh. In all the computations, the maximum number of shells is 5 for the two molecules. Only the three first ones seem to be relevant. This proves that the value of τ_R results from the contribution of all these τ_{Ri}. In general, τ_{Ri} has a much smaller value than the value of τ_R because the constraint to remain in i shells simultaneously is much greater than to remain at least one shell and because a molecule can go from one class i to another without leaving the ammonium neighborhood. For each sample, the maximum value is in red color. However, sometimes the maximum value may have the same order of magnitude as τ_R (the values are in blue color). This happens mostly for τ_{R3} and τ_{R4} with WU = 10% and T = 300 K. This comes from the highest contribution of the long residence time. For instance, if all the molecules, remaining at least in one shell during 100 ns, stay in fact in i shells during this time, τ_{Ri} must be greater than τ_R because the number of molecules staying at least in one shell is greater than the number of molecules staying in i shells. In other word, the contribution of these sticking molecules in τ_{Ri} is higher.

In most cases, τ_{Ri}^{Ow} and τ_{R1}^{Oh} are a decreasing function of T and WU as τ_R. We can also observe that at T = 300 K τ_{R2}^{Ow} , τ_{R1}^{Oh}

Please cite this article as: Magnico P, Molecular dynamics study on water and hydroxide transfer mechanisms in PSU-g-alkyl-TMA membranes at low hydration: Effect of side chain length, International Journal of Hydrogen Energy, https://doi.org/10.1016/j.ijhydene.2021.07.081

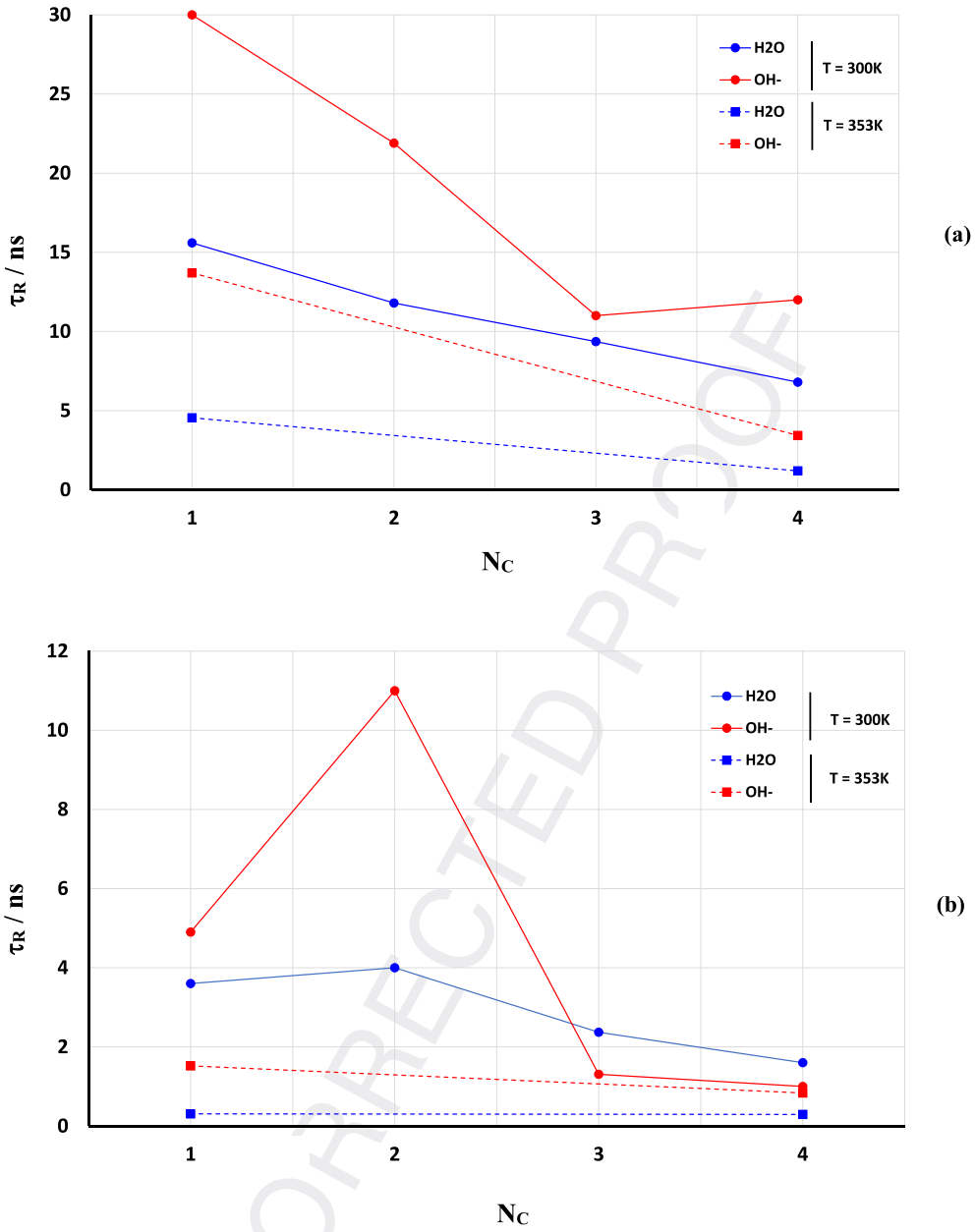

Fig. 5 – Mean residence time in the ammonium shell vs. the number of carbon atom in the alkyl chain. (a): WU = 10%; (b): WU = 20%.

and τ_{R2}^{Oh} have the highest value in most of the simulations which is consistent with the values of N-Oh CN. However, if T = 353 K, τ_{R2} and τ_{R3} have the highest value. As N_C increases, τ_{R2}^{Oh} shows a maximum for ETMA ($N_C = 2$) unlike τ_{R2}^{Ow} which is a decreasing function.

At T = 300 K, the mean number of QA shells (N_{shell}) in which the water molecules enter is 4 and 9 if WU = 10% and 20% respectively, whereas the OH enters in 4 shells for the two WU values. At T = 353 K, it increases moderately to 7 for H_2O if WU = 10%. But a jump at this temperature is observed when WU increases to 20%: the number of shell increases to 27 and to 7 for H_2O and OH respectively. So, the increase of N_{shell}^{Ow} with T or WU follows the decrease of τ_R^{Ow}. However, this is not observed for OH for which N_{shell} is independent of WU at T = 300 K.

Van Hove function

In relation with the high value of the correlation time, the Van Hove function $g_{vh}(r,t)$ allow to evaluate how long the system keep the memory of the initial configuration. $g_{vh}(r,t)$ is the probability density of finding a particle i in the vicinity of r at time t, knowing that a particle j is in the vicinity of the origin at time t = 0:

$$g_{vh}(r,t) = \frac{1}{N_j}\sum_{i=1}^{N_i}\sum_{j=1}^{N_j}\delta(r - r_i(t) + r_j(0)) \quad (5)$$

where N_i and N_j is the number of particles i and j respectively. If the two particles are of the same kind, two Van Hove functions can be computed: the self one $g_{vh,s}(r,t)$ if $i = j$ and the

Please cite this article as: Magnico P, Molecular dynamics study on water and hydroxide transfer mechanisms in PSU-g-alkyl-TMA membranes at low hydration: Effect of side chain length, International Journal of Hydrogen Energy, https://doi.org/10.1016/j.ijhydene.2021.07.081

distinct one $g_{vh,d}(r,t)$ if $i \neq j$. $g_{vh,s}(r,t)$ is the probability that a particle has moved a distance r in time t. It is related to the diffusion process. $g_{vh,d}(r,0)$ is the common radial distribution function $g(r)$.

Fig. 6 shows the variation in time of the N-Ow and N-Oh distinct Van Hove function for MTMA (WU = 20%) at T = 300 K. At time t = 1 ps, the profiles are close to the correlation ones in Fig. 3. The main peak expands a little and the secondary one becomes a shoulder after 50 ns. This means that the time relaxation is much greater than 100 ns. The relaxation time is the time needed for an ammonium group to be exchanged with a water molecule or a hydroxide ion. This relaxation time scale can be explained by comparing the MSD and the size of the ammonium group. At time t = 100 ns, the MSD is around 70 $Å^2$ (i.e if we take into account of all the data 1ns after the annealing process), which is equivalent to a displacement radius of $0.5 \times \sqrt{70} \approx 4$ Å. From the 1st peak of $g_{N-Oh}(r)$ and $g_{N-Ow}(r)$ we can estimate that the radius of the ammonium group is around 3 Å. So, the small displacement radius of the ammonium group comparable to its radius does not allow the OH ions and the H_2O molecules to replace the ammonium groups.

The profiles of Ow and Oh $g_{vh,s}(r,t)$ in Fig. 7 show that even after 10 ns the molecules remain inside a cage of neighboring molecules. But this time Ow et Oh have not the same behavior. As concerns Ow, the position of the peak remains at 0.55 Å. At 500 ps a shoulder appears and becomes a 2nd peak located at 3 Å until t = 8 ns. The profile expands over the distance of 4 Å. Then this maximum moves away after 15 ns. The 1st peak disappears after 50 ns with a characteristic time of 7 ns. So, the figure shows a cage effect and a hopping process at short distance and a kind of diffusive one at long distance and time greater than 3 Å and 15 ns respectively. In the case of a homogeneous liquids, the profile is a gaussian curve moving away revealing a Fickian process with no cage effect [71–73]. Cage and hopping phenomena are usually observed in

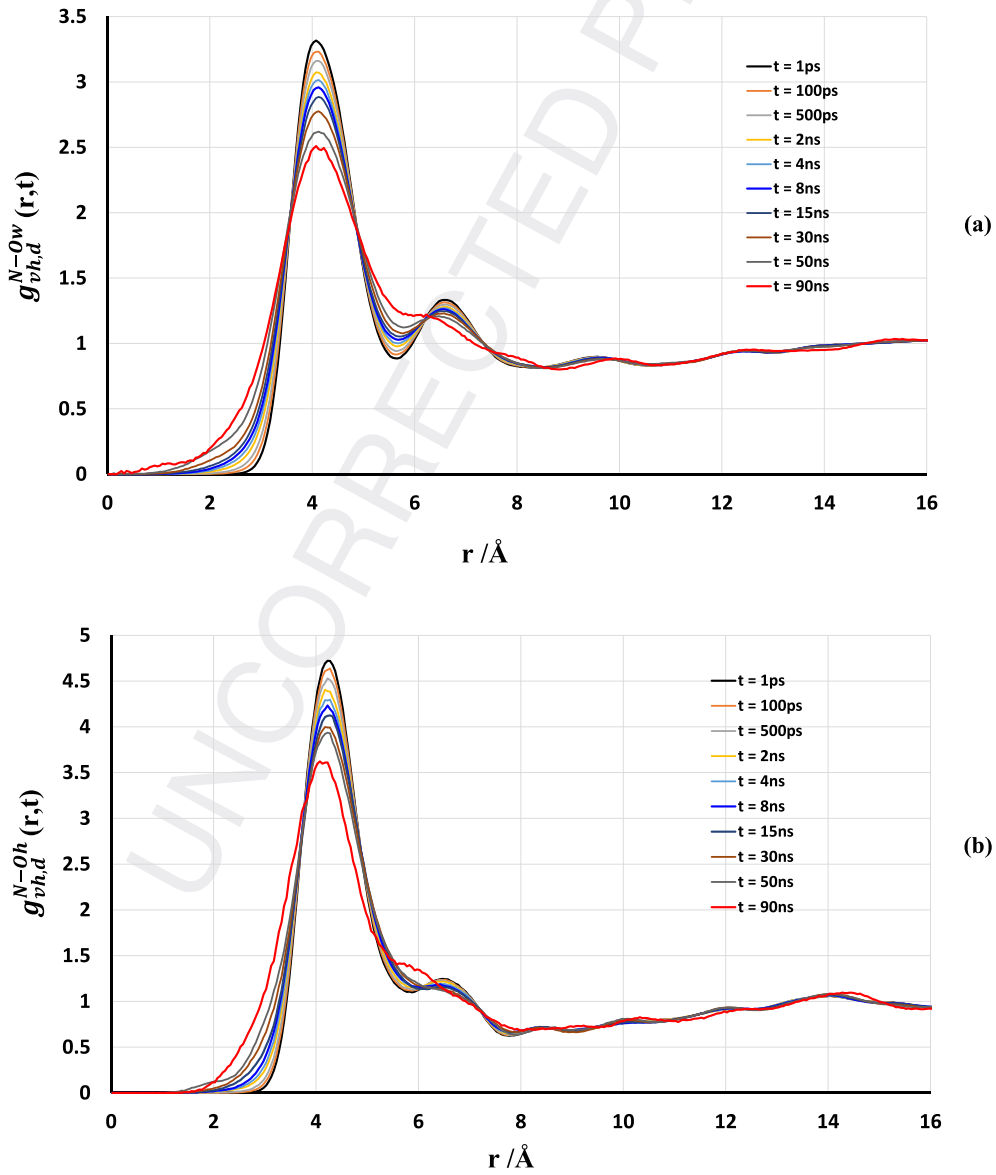

Fig. 6 – Distinct Van Hove function at different times. MTMA (WU = 20%, T = 300 K). (a): N-Ow; (b): N-Oh.

Please cite this article as: Magnico P, Molecular dynamics study on water and hydroxide transfer mechanisms in PSU-g-alkyl-TMA membranes at low hydration: Effect of side chain length, International Journal of Hydrogen Energy, https://doi.org/10.1016/j.ijhydene.2021.07.081

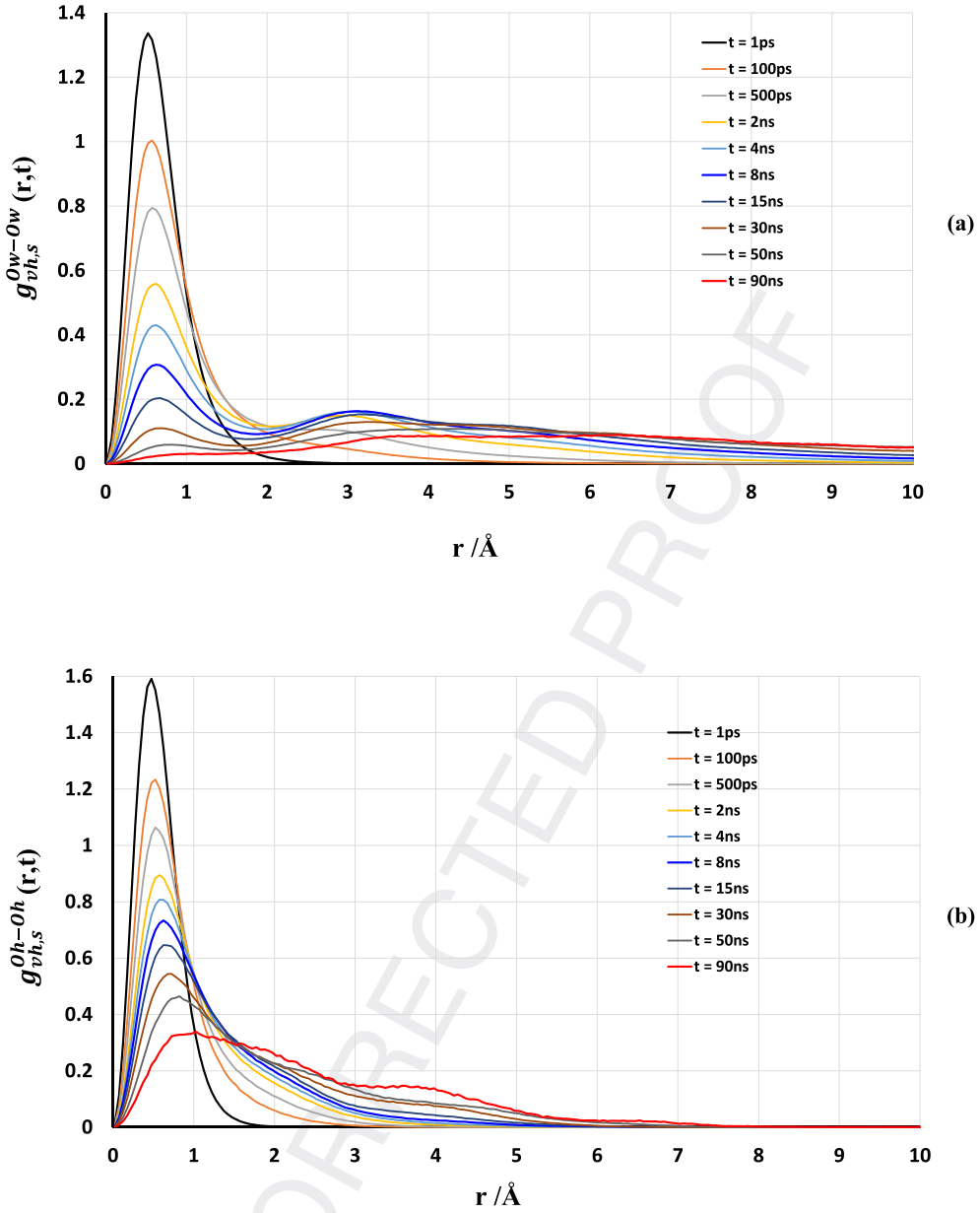

Fig. 7 – Self Van Hove function at different times. MTMA (WU = 20%, T = 300 K). (a): Ow-Ow; (b): Oh-Oh.

supercooled media, and also observed in the hydration shell of proteins or of sulfonate anions in Nafion eventually [74–78]. As concerns the hydroxide ion, the cage effect is more pronounced even if the peak moves slightly from 0.48 Å to 0.9 Å (the characteristic time is much greater than 20 ns). No shoulder is present until 50 ns. In order to get an idea of the distance travelled by a molecule in homogeneous fluid, it can be computed from the maximum position of the Gaussian distribution. For instance, at T = 300 K, $D_{H2O} \approx 2 \times 10^{-5}$ cm^2/s a water molecule needs 30 ps to travel 5 Å. In this work, the diffusion coefficients lye between 10^{-8} cm^2/s and 10^{-7} cm^2/s. To travel the same distance a molecule needs 6.5 ns and 0.65 ns respectively.

Figs. SI-04 and 05 show the same Van Hove functions but at 353 K. The temperature effect is mainly noticeable for the self-correlations. For H_2O, the 1st peak of the self-function remains at the same place while the 2nd peak appearing after 100 ps moves and expands after 500 ps. So, we can approximately estimate that the relaxation time is around 15 ns, time after which the 1st peak disappears. As concerns the Oh self-function, the peak moves from 0.63 Å to 2.4 Å without any shoulder before 8 ns. Even if the Oh profiles are not gaussian, a translational diffusion begin to appear, which is not the case for Ow. All these observations are consistent with the high decrease of τ_R as T increases. Fig. SI-04 show that the radial correlation between the ammonium group and H_2O begin to disappear at very long time. But the correlation remains for OH. This reveals that the effect of the small displacement of N is persistent. As WU decreases to 10%, the same profiles are observed but shows a smaller dependence on time, i.e the time relaxation is a decreasing function of WU. The dependence on N_C of the time evolution of $g_{vh,s}$ is observable mostly

Please cite this article as: Magnico P, Molecular dynamics study on water and hydroxide transfer mechanisms in PSU-g-alkyl-TMA membranes at low hydration: Effect of side chain length, International Journal of Hydrogen Energy, https://doi.org/10.1016/j.ijhydene.2021.07.081

if WU = 20% and the sensitivity increases with T. As shown Fig. SI-06 (BTMA (WU = 20% T = 353 K)), the hopping and the diffusion process are faster than with MTMA in accordance with the decrease with τ_R and the increase of D_{oh} with N_C.

Neighborhood structure of Ow and Oh

The cage effect and the presence of a 2nd peak is related to the neighborhood of Ow and Oh. The radial position of this peak is close to the 1st peak one of the radial distributions Ow-Ow and Ow-Oh. In order to investigate this region, the neighbor radial profiles are shown in Fig. 8 (MTMA − WU = 20%, T = 300 K). The profiles are computed in the following way. At each time step and for each atom Ow or Oh, their neighbors are ordered in function of the radial distance in a vector. One vector is used for each atomic species. Then the radial distance of the jth neighbor is averaged over the time interval (5 ns in the present work). The probability for an atom of species i to be the jth neighbor of Ow or Oh is normalized by the total number of the jth neighbor atoms found over the time interval. So, from left to right in Fig. 8(a), the 1st points of each atomic species at 2.18 Å represent the 1st neighbors, the 2nd points at 2.36 Å are the 2nd neighbors and so on. The distance between two successive neighbors is not constant. The mean radial position is defined with an average variability of ±0.5 Å for Ow and of ±0.3 Å for Oh. The atom Q4 represents the ghost atom of the water model located at 0.155 Å from Ow and has a partial charge of −1.112. Hx is the hydrogen atom of the ammonium group. Ha and Ca are the hydrogen and the carbon atoms of the aromatic ring in the PSU backbone respectively.

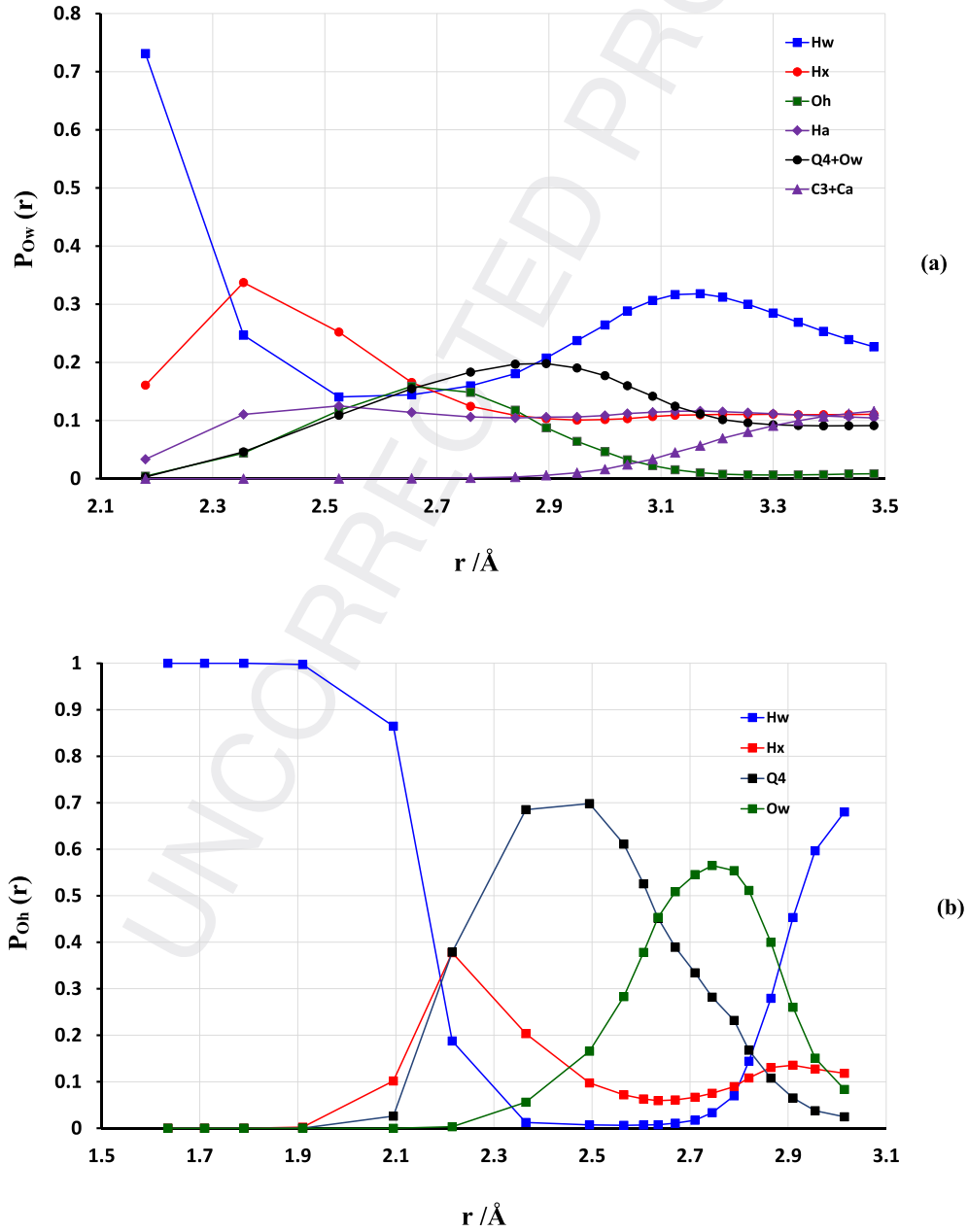

Fig. 8 − Probability of finding an atomic species at a distance r of: (a) Ow; (b) Oh. MTMA (WU = 20%, T = 300 K).

Please cite this article as: Magnico P, Molecular dynamics study on water and hydroxide transfer mechanisms in PSU-g-alkyl-TMA membranes at low hydration: Effect of side chain length, International Journal of Hydrogen Energy, https://doi.org/10.1016/j.ijhydene.2021.07.081

C3 refers to the carbon atom of the methyl groups in the backbone and in the spacer.

Fig. 8(a) shows the species composition of the Ow neighbors. The curves of Q4 and Ow are put together in the same one because they are close to each other. It must be noticed that the radial position of the maxima of the main species is close to the position of the 1st peak of the RDF and their height results from the computation of the probability over all the species present at the jth neighbor position. As the radial distance increases from 2.1 Å, the Hw and Hx are the main neighbors, the probability to find an atom Ha increases to the asymptotic value of 12% at 2.5 Å. The probability to find an oxygen atom increases to a value of 15% and 20% for Ow and Oh respectively. The maxima are explained by the presence of water-water (ww) and water hydroxide (wh) hydrogen bond (HB). Beyond a radial distance of 3 Å, the three species Hx, Ha, Ow and the aromatic carbon Ca are equiprobable. At the same time, the main species Hw reaches a maximum of 32% at 3.15 Å which is related to a 2nd hydration shell. So, the water molecule moves also in the vicinity of the backbone. The carbon and the nitrogen atoms of the ammonium group and Hh also do not appear because the number of these atoms are small compared to Hw and the nitrogen atom is also too far away.

As WU decreases to 10%, the same kind of profiles is observed with a much less contribution of Hw and of Ow. Hx is the main neighbor at a radial distance r < 2.6 Å. The probability of finding Hw, Oh and Ha increases with r, so that at r > 2.8 Å, Hx, Hw and Ha are equiprobable (15%). The Oh probability

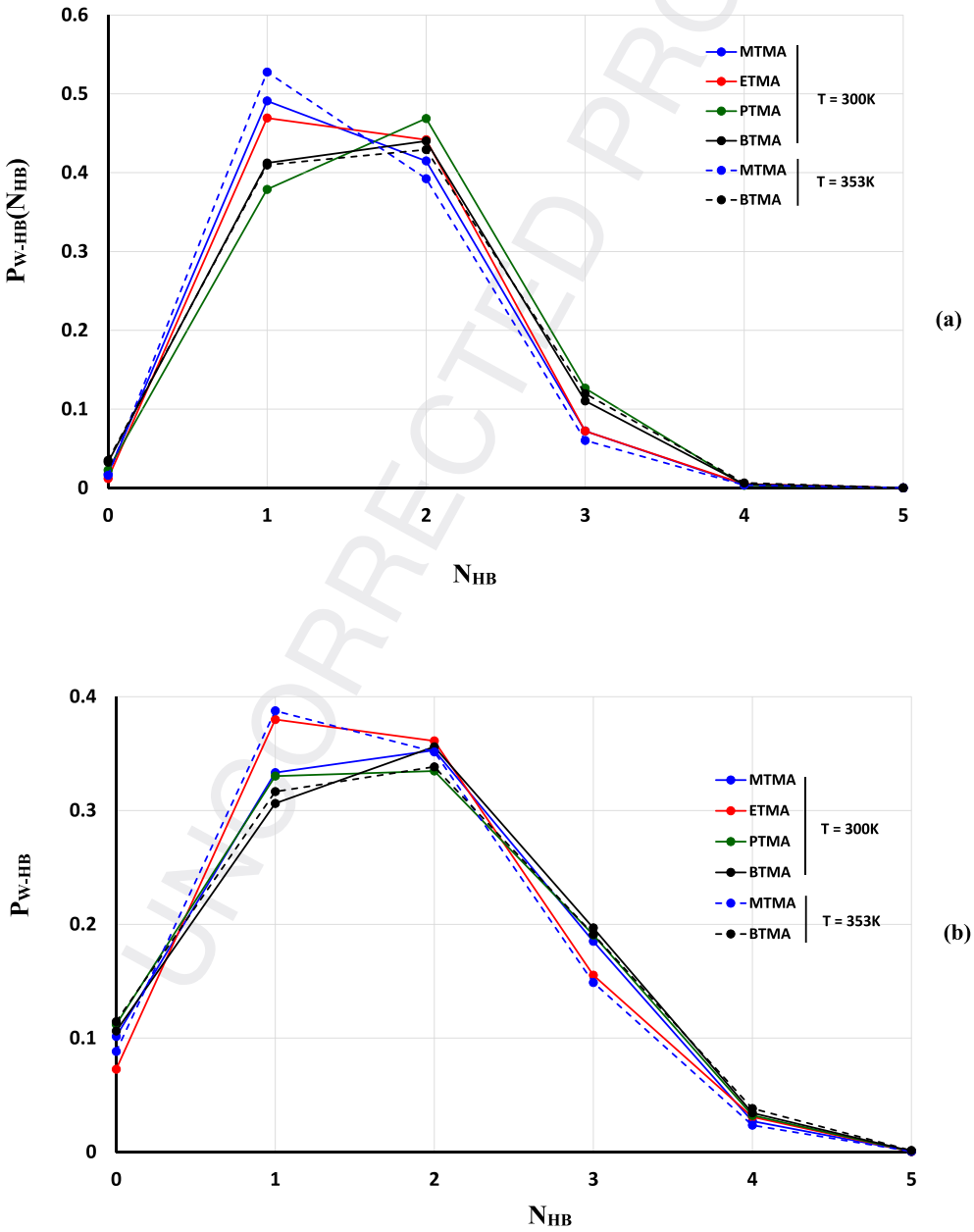

Fig. 9 – Probability that a water molecule forms N_{HB} with other water molecules and hydroxide ions. (a): WU = 10%; (b): WU = 20%.

Please cite this article as: Magnico P, Molecular dynamics study on water and hydroxide transfer mechanisms in PSU-g-alkyl-TMA membranes at low hydration: Effect of side chain length, International Journal of Hydrogen Energy, https://doi.org/10.1016/j.ijhydene.2021.07.081

curve have a maximum at 2.7 Å and its value decreases strongly after 2.7 Å. At r > 3 Å, the Ca probability curve meets the three last ones. The minimum of the Ow $g_{vh,s}(r,t)$ profiles at around 1.8–2 Å correspond to the position of the three first neighbors (Hw, Hx, Ha) considering the variability of the radial position of these neighbors. The 2nd peak in Fig. 7(a) corresponds to the maximum of the probability of finding another Ow atom in the vicinity of Ow. The spacer length has a small effect on the neighbor distribution around Ow. For BTMA, the slight decrease of the contribution of Ha and Ca is balanced by the increase of the spacer hydrogens contribution.

As concerns Oh, its neighbors are the atoms Hw, Hx and Ow only. So, the OH ions remain far away from the PSU backbone and the spacer, and the distribution around Oh does not depend on the spacer length. The maximum of Hx and Ow curves appear successively at 2.2 Å and 2.8 Å. As we will see in the next section, the OH ions are bonded to several water molecules so that the OH ions are separated from the Hx atoms by the Hw atoms which occupy all the volume in close contact with Oh. Owing to its partial charge, Q4 has a higher interaction with Hw than Ow (Ow has no partial charge). Therefore, the maximum of Q4 is located at a radial position smaller than the Ow maximum. This is an artefact of the water model. As for Ow, Hw is also the main neighbor at long distance (r > 2.7 Å) revealing a second hydration shell. As WU decreases to 10%, all the maximum remains at the same radial position. The height of the maximum of Hx curve increases at the same time to a value of 0.57 as the volume occupied by Hw atoms decreases. The presence of Hw at a distance lower than 2.1 Å is related to the hydrogen bond formation between OH and H_2O. The Oh and Hh atoms are not present because they are too far away (see Table SI_1(a)). We will see that the OH forms 3.5 to 5 HB with H_2O. So, the H_2O are localized around the OH [26,31,32,79] and this geometry avoids the OH to be close to Hx. Owing to the presence of the hydrogen bonds with H_2O, the OH ions tend to diffuse with the H_2O as the peak of $g_{vh,s}(r,t)$ extends with time. But at the same time electrostatic interaction with the ammonium group prevent the OH to move away and this peak remains at the same place when T = 300 K. At 353 K, the kinetic energy is high enough for OH to be less influenced by the ammonium group and to initiate a real but small diffusion process.

Hydrogen bond network

The structural organization of aqueous phase is analyzed by considering the hydrogen bond network. It is common to use the geometric criterion to define the hydrogen bond. Luzar and Chandler [80] used a distance of 2.5 Å between the hydrogen and the oxygen atoms, a distance of 3.5 Å between two oxygen atoms of two different water molecules and an angle of 30° between the three atoms $Hw\widehat{Ow}Ow$. The clusters are identified by means of the Stoddart algorithm [81]. Huo et al. [82] observed that these three values must be recalculated in their membrane systems. In ppo-g-imidazole, the distance Ow-Ow and Ow-Hw is 4.45 Å and 2.35 Å respectively, and the angle is 40°. In order to take into account of the interaction OH/H_2O, the authors defined three other criteria: 3.45 Å and 2.35 Å for the distance Oh-Ow and Oh-Hw respectively and an angle of 30°. These new values correspond to the radial position of the first shell and to the angle distribution between the three atoms $Hw\widehat{Ow}Ow$ and $Hw\widehat{Ow}Oh$. Fig. SI-02 agree with these distance criteria. Fig. SI-07 shows the angle distribution of the water/water and water hydroxide pairs in MTMA and BTMA with WU = 10% and 20%. The distribution is independent of T. As in Ref. [79] a shoulder is observed if WU = 10% which justifies these authors to increase the value of $Hw\widehat{Ow}Ow$ to 40°.

In the present work, the mean cluster size, i.e the number of water molecules bonded to each other (N_{CL}), varies between

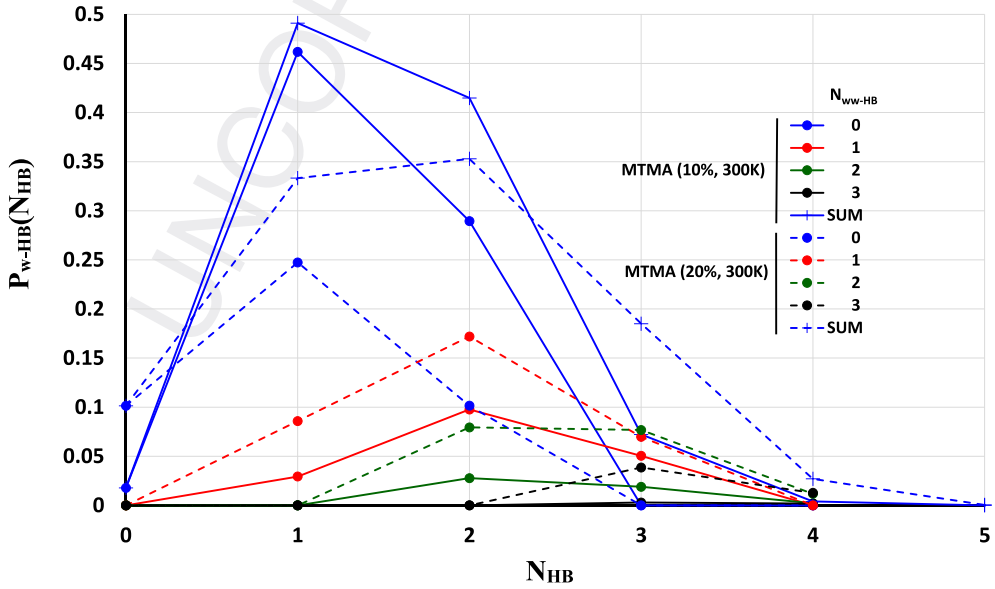

Fig. 10 – Probability that a water molecule forms N_{HB} with other water molecules and hydroxide ions for an imposed value of N_{WW} bond to others H_2O. The SUM curves are the profiles in Fig. 9.

Please cite this article as: Magnico P, Molecular dynamics study on water and hydroxide transfer mechanisms in PSU-g-alkyl-TMA membranes at low hydration: Effect of side chain length, International Journal of Hydrogen Energy, https://doi.org/10.1016/j.ijhydene.2021.07.081

2.1 and 2.5 at T = 300 K and 353 K depending on WU: 75% and 25% for two and three H_2O respectively if WU = 10% and 60% and 30% if WU = 20%. At WU = 20%, the cluster of size 4 represents 7%. Depending on N_C, the isolated H_2O varies from 1.1% to 3.5% and from 7% to 11% when WU = 10% and 20% respectively. The proportion of H_2O bonded to one OH at least varies from 66% to 75% and from 30% to 39% when WU = 10% and 20% respectively. This means that all the OH are bonded to a water molecule. The number of HB per OH varies from 3.5 and to 5 when WU = 10% and 20% respectively. These statistics are independent of T. Huo et al. [79] find values of 2.5 and 4.5 with the same criteria for the same number of H_2O per OH. In Ref. [32], the computed values are 3.3 and 4.5.

Fig. 9 show the probability ($P_{W\text{-}HB}$) that a water molecule forms N_{HB} hydrogen bond with water molecules (ww-HB) and with hydroxide ions (wh-HB) for all the systems studied at T = 300 K and 353 K. In the following, the H_2O which are not bonded to another water molecule are included in the cluster category. So, $P_{W\text{-}HB}$ ($N_{HB} = 0$) represents the probability that a water molecule is isolated. These profiles are similar to the profile computed by Huo et al. [79] with $\lambda_N = 3$ and 6. For these values of λ_N, the number of H_2O per OH in their system is 2 and 5 respectively a bit smaller than the values used in the present work. We see that the distribution expands with WU and shows little sensitivity to T. If WU = 10%, $P_{W\text{-}HB}$ ($N_{HB} = 1$) decreases with the spacer length from $N_C = 1$ to 3 unlike $P_{W\text{-}HB}$ ($N_{HB} = 2$). If WU = 20%, $P_{W\text{-}HB}$ is not sensitive to N_C but in the case ETMA.

In order to go further in the analysis, the probability for a water molecule to form N_{WH} HB in function of N_{HB} (N_{WW} + N_{WH}) with N_{WW} fixed is plotted in Fig. 10 for the two systems MTMA WU = 10% and 20% at 300 K. N_{WW} and N_{WH} mean the number of HB between two water molecules and between a water molecule and a hydroxide ion respectively. Each curve represents a fixed value of N_{WW}. For example, if

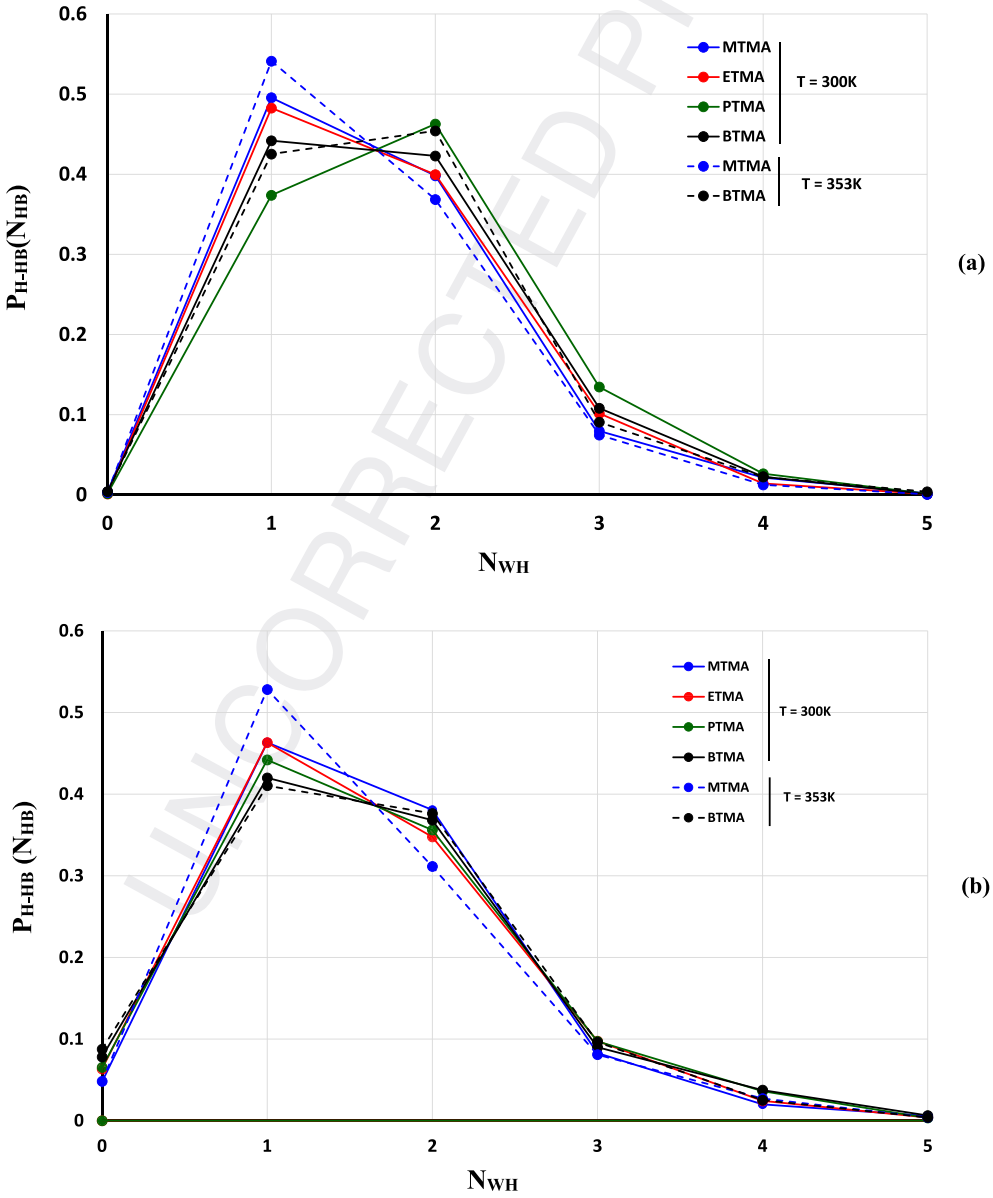

Fig. 11 – Probability that, in a cluster, hydroxide ions form N_{WH} HB with water molecules. (a): WU = 10%; (b): WU = 20%.

Please cite this article as: Magnico P, Molecular dynamics study on water and hydroxide transfer mechanisms in PSU-g-alkyl-TMA membranes at low hydration: Effect of side chain length, International Journal of Hydrogen Energy, https://doi.org/10.1016/j.ijhydene.2021.07.081

$N_{WW} = 1$ (blue curve) and $N_{HB} = 1$ then $N_{WH} = 0$, if $N_{HB} = 2$ then $N_{WH} = 1$ and so on. The curves with crosses represent the sum of all the probabilities at a fixed value of N_{HB} as in Fig. 9. We observe that the probability for a water molecule to form one and even two wh-HB only (blue curve) is very high. These two configurations represent the main configuration. This is observed for the three other polymers. In particular for PTMA, the maximum of $P_{W\text{-}HB}$ is located at $N_{HB} = 2$. This comes mainly from the small probability for the configuration H_2O–OH and a quite high probability for the configuration HO–H_2O–OH to exist. As WU increases to 20%, the probability for H_2O to form no ww-HB ($N_{WH} \geq 1$) decreases a lot unlike the probability for H_2O to form at least one ww-HB (red and green curves). For $N_{HB} = 2$, the configuration H_2O–H_2O–OH largely replaces the configuration HO–H_2O–OH. The balance between these two configurations is revealed by the small decrease of the SUM curve at $N_{HB} = 2$. This balance is observed for ETMA and BTMA but not for PTMA. For $N_{HB} = 3$, the increase of Pw-HB is induced by the increase of the ww-HB, i.e the increase of the cluster size. The main configurations are OH–$H_2O(-H_2O)_2$ and $(OH-)_2H_2O$–H_2O. The profiles are independent of T whatever WU and N_C. We can conclude that the high decrease of the number of H_2O forming no ww-HB, revealing the increase of the connectivity, does not induce an increase of D_{Ow} for MTMA, ETMA and BTMA (Fig. 4), and that the high sensitivity of D_{Ow} with T (WU = 20%) is in contradiction with the small sensitivity of the ww-HB/wh-HB repartition. The sensitivity of T is

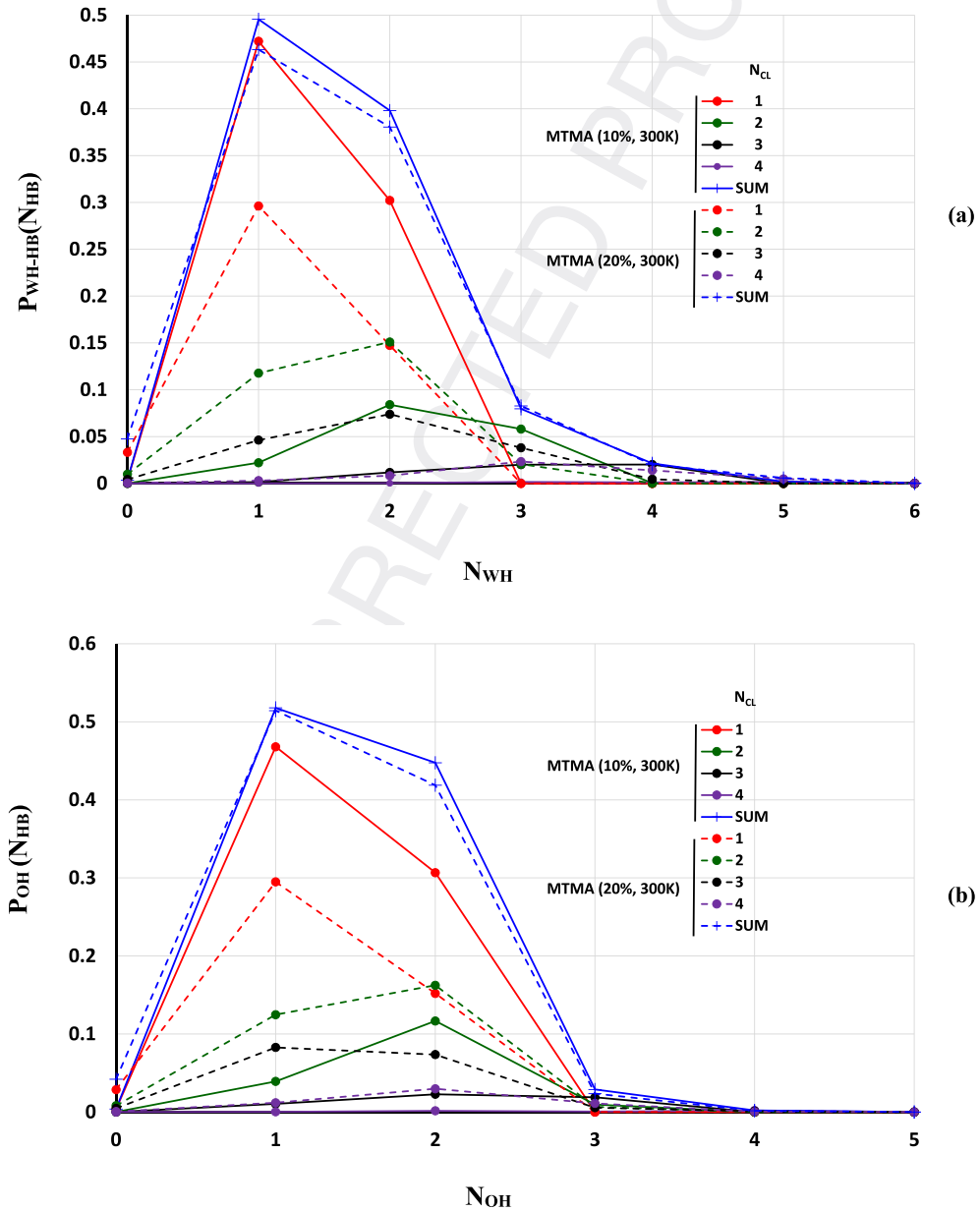

Fig. 12 – Probability that (a): hydroxide ions form N_{WH} HB with a cluster containing N_{CL} water molecules. The SUM curves are the profiles in Fig. 10; (b): N_{OH} hydroxide ions are bonded to cluster containing N_{CL} water molecules. The SUM curves represent the probability that N_{OH} hydroxide ions are bonded to a cluster.

Please cite this article as: Magnico P, Molecular dynamics study on water and hydroxide transfer mechanisms in PSU-g-alkyl-TMA membranes at low hydration: Effect of side chain length, International Journal of Hydrogen Energy, https://doi.org/10.1016/j.ijhydene.2021.07.081

related to the increase of the Brownian motion. In this case there might be a threshold value of WU under which the temperature dependence is small. We can observe also that the variation of Pw-HB with N_C at $N_{HB} = 1$ and 2 (WU = 10%, T = 300 K) follows the variation of D_{Ow}.

The HB network between the clusters and the hydroxide ions is analyzed now. The probability that water molecules in a cluster forms N_{WH} hydrogen bonds with OH ions is displayed in Fig. 11. All the samples are represented for T = 300 K and 353 K. At the origin ($N_{WH} = 0$) the clusters are not bonded to a hydroxide ion. The two figures look quite similar to Fig. 9. The maximum number of wh-HB in a cluster is 4 whatever the value of WU, T, and N_C. As observed in Fig. 9 in the case WU = 10%, the number of clusters forming one wh-HB, i.e bonded to one OH, decreases with N_C until $N_C = 3$ (PTMA), but the number of clusters forming two wh-HB reaches a maximum for PTMA. The sensitivity to T is also small. If WU = 20%, the probability is slightly sensitive to N_C and T but MTMA.

As above, let us analyze the probability in function of the cluster size. In Fig. 12(a), each curve with filled circles represents the probability for a fixed cluster size. The two curves with crosses represent the sum of the probabilities at a fixed value of N_{WH}. As before, when WU = 10%, the OH are mainly bonded to clusters constituted of one H_2O. As WU increases for a fixed value of N_{WH}, the probability of the two configurations H_2O–OH (P_{HB1}) and OH–H_2O–OH (P_{HB2}) (red curves) decreases to the benefit of clusters of greater size (green and black curves) keeping constant the probability for a cluster to form N_{WH} HB (blue curves). In other word, the global probability profile is not sensitive to WU. This last observation is not observed with PTMA owing to high decrease of the probability of the configuration OH–H_2O–OH: despite the increase of the cluster size, the most important configuration remains H_2O–OH. This leads to the displacement of the maximum from $N_{WH} = 2$ to $N_{WH} = 1$. All these results are slightly dependent on T.

Does one OH forms one or more HB with a cluster? Fig. 12(b) displays the probability that a cluster of size N_{CL} is bonded to N_{OH}. The similarity with Fig. 12(a) proves that each OH have about one HB per cluster but for $N_{WH} = 3$. For $N_{CL} > 2$, one OH can form 2 bonds. However, the number of wh-HB per OH is roughly the number of HB with clusters which size ranges from 1 to 4.

At this step of the analysis, a tentative of explanation may be suggested about the decrease of D_{Oh} and D_{Ow} as WU increases in the case of MTMA at T = 300 K. This behavior may be related to the contribution WH hydrogen bond network if we consider that the clusters formed by N_{CL} H_2O diffuses less than the clusters formed of (N_{CL}-1) H_2O. The above observations about Fig. 12(a) may leads to the same conclusion about the decrease of D_{Oh} and of D_{Ow} with N_C if WU = 10% and T = 300 K. Of course, other mechanisms such as the motion through the ammonium group network or the articulation of the side chain may occur with an influence level depending on the spacer length.

Conclusion

Under very small hydration conditions, D_{Ow} and D_{Oh} is so small that they have mostly the same order of magnitude as D_N at T = 300 K. At WU = 10% ($\lambda_N = 3$), the hierarchy ($D_{Ow} > D_{Oh} > D_N$) is not always observed and the diffusivity seems to be unsensitive to the temperature. This can be explained by a WU threshold which value depends on the molecular species and on N_C. Owing to the small diffusivities and the fluctuation of the MSD, no correlation of D with N_C is observed but for D_{Ow} at WU = 20% ($\lambda_N = 6$) which is an increasing function of N_C. Membranes with higher values of λ_N and N_C must be studied.

The investigation of the residence time distribution around a quaternary ammonium group (QA) shows that the characteristic times τ_R^{Ow} and τ_R^{Oh} decrease with N_C, WU and T. Its typical value lies from 1 ns to 30 ns at T = 300 K and from 0.3 ns to 15 ns at 353 K with $\tau_R^{Oh} > \tau_R^{Ow}$. The OH and H_2O may stay inside until three QA group shells simultaneously. This confirms that these molecules spend most of the time in the vicinity of QA groups. Owing to the high volume occupied by the QA groups, the Van Hove distinct correlation functions show that the correlation between the QA group and the OH and H_2O remains important over 100ns even at 353 K.

The self Van Hove functions of Ow and Oh reveal a Brownian motion inside a cage formed by the nearest atoms and a hopping motion. For H_2O at T = 300 K, the cage effect is present during all the simulation time. The hopping motion appear after 500 ps with a 2nd peak located at 3 Å. This peak begins to move and expanses after 20 ns revealing a diffusion process observed also at T = 353 K with smaller characteristic times. For OH at T = 300 K, a quite hopping process appears after 50 ns. However, at T = 353 K the non-gaussian distribution of displacement moves and expands so that the maximum is located at 2.5 Å at 90 ns. It seems that at T = 353 K these times decrease with N_C.

Finally, the connectivity of the hydrogen bond (HB) network is explored. As the hydration number is very small ($\lambda_N = 3$), most of water molecules form at most one bond with other water molecules. As WU increases, the number of water-water and hydroxide-water HB increase. The main bond configurations OH–H_2O and OH–H_2O–OH is partially replaced by H_2O–H_2O and $(H_2O)_2$–OH respectively. As concerns the OH ion, the main bond configurations OH–H_2O and OH–H_2O–OH is partially replaced by $(H_2O)_2$–OH and by OH–$(H_2O)_2$–OH and OH–$(H_2O)_3$–OH. The amount of replacement depends on N_C mainly when WU = 10%.

The simulations show counterintuitive results as concerns MTMA as concerns the decrease of diffusivity as WU increases. However, no specific signs on the membrane structure are revealed nor by the radial correlation function nor by the spatial repartition of the functional groups. So, a deeper analysis of transfer efficiency through the ammonium shells under drastic condition will be carried out in a future work.

Please cite this article as: Magnico P, Molecular dynamics study on water and hydroxide transfer mechanisms in PSU-g-alkyl-TMA membranes at low hydration: Effect of side chain length, International Journal of Hydrogen Energy, https://doi.org/10.1016/j.ijhydene.2021.07.081

Declaration of competing interest

The authors declare that they have no known competing financial interests or personal relationships that could have appeared to influence the work reported in this paper.

Acknowledgement

Q4

Centre de Calcul Intensif d'Aix-Marseille is acknowledged for granting access to its high performance computing resources.

Appendix A. Supplementary data

Supplementary data to this article can be found online at https://doi.org/10.1016/j.ijhydene.2021.07.081.

REFERENCES

[1] Ran J, Wu L, He Y, Yang Z, Wang Y, Jiang C, Ge L, Bakangura E, Xu T. Ion exchange membranes: new developments and applications. J Membr Sci 2017;522:267–91.
[2] Hong JG, Zhang B, Glabman S, Uzal N, Dou X, Zhang H, Wei X, Chen Y. Potential ion exchange membranes and system performance in reverse electrodialysis for power generation: a review. J Membr Sci 2015;486:71–88.
[3] Mei Y, Tang CY. Recent developments and future perspectives of reverse electrodialysis technology: a review. Desalination 2018;425:156–74.
[4] Weber AZ, Mench MM, Meyers JP, Ross PN, Gostick JT, Liu Q. Redox flow batteries: a review. J Appl Electrochem 2011;41:1137–64.
[5] Kusoglu A, Weber AZ. New insights into perfluorinated sulfonic-acid ionomers. Chem Rev 2017;117:987–1104.
[6] Dekel DR. Review of cell performance in anion exchange membrane fuel cells. J Power Sources 2018;375:158–69.
[7] Fang J, Wu Y, Zhang Y, Lyu M, Zhao J. Novel anion exchange membranes based on pyridinium groups and fluoroacrylate for alkaline anion exchange membrane fuel cells. Int J Hydrogen Energy 2015;40:12392–9.
[8] Wang H, Du X, Zhang H, Shen H, Liu Q, Wang Z. Synthesis and characterization of long-side-chain type quaternary ammonium-functionalized poly(ether ether ketone) anion exchange membranes. Int J Hydrogen Energy 2021;46:8156–66.
[9] Park CH, Kim T-H, Kim DJ, Nam SY. Molecular dynamics simulation of the functional group effect in hydrocarbon anionic exchange membranes. Int J Hydrogen Energy 2017;42:20895. 20203.
[10] Arges CG, Zhang L. Anion exchange membranes' evolution toward high hydroxide ion conductivity and alkaline resiliency. ACS Appl Energy Mater 2018;1:2991–3012.
[11] Wang X, Li Z, Qu Y, Yuan T, Wang W, Wu Y, Li Y. Review of metal catalysts for oxygen reduction reaction: from nanoscale engineering to atomic design. Inside Chem 2019;5:1486–511.
[12] Vij V, Sultan S, Harzandi AM, Meena A, Tiwari JN, Lee W-G, Yoon T, Kim KS. Nickel-based electrocatalysts for energy-related applications: oxygen reduction, oxygen evolution, and hydrogen evolution reactions. ACS Catal 2017;7:7196–225.
[13] Wu G, Zelenay P. Nanostructured nonprecious metal catalysts for oxygen reduction reaction. Accounts Chem Res 2013;46:1878–89.
[14] Gottesfeld S, Dekel DR, Page M, Bae C, Yan Y, Zelenay P, Kim YS. Anion exchange fuel cells: current status and remaining challenges. J Power Sources 2018;375:170–84.
[15] Varcoe JR, Atanasov P, Dekel DR, Herring AM, Hickner MA, Kucernak PA, Mustain WE, Nijmeijer K, Kohl PA, Scott K, Xu T, Zhuang L. Anion-exchange membranes in electrochemical energy systems. Energy Environ Sci 2014;7:3135–91.
[16] Tao Z, Wang C, Zhao X, Li J, Guiver MD. Progress in high-performance anion exchange membranes based on the design of stable cations for alkaline fuel cells. Adv Mater Technol 2021;6:2001220.
[17] Zhang X, Li S, Chen P, Fang J, Shi Q, Weng Q, Luo X, Chen X, An Z. Imidazolium functionalized block copolymer anion exchange membrane with enhanced hydroxide conductivity and alkaline stability via tailoring side chains. Int J Hydrogen Energy 2018;43:3716–30.
[18] Wang C, Tao Z, Zhou Y, Zhao X, Li J, Ren Q, Guiver MD. Anion exchange membranes with eight flexible side-chain cations for improved conductivity and alkaline stability. Sci China Mater 2020;63:2539–50.
[19] Zhang X, Li S, Chen P, Fang J, Shi Q, Weng Q, Luo X, Chen X, An Z. Imidazolium functionalized block copolymer anion exchange membrane with enhanced hydroxide conductivity and alkaline stability via tailoring side chains. Int J Hydrogen Energy 2018;43:3716–30.
[20] Jin C, Zhang S, Cong Y, Zhu X. Highly durable and conductive poly(arylene piperidine) with a long heterocyclic ammonium side-chain for hydroxide exchange membranes. Int J Hydrogen Energy 2019;43:24954–64.
[21] Oh BH, Kim AR, Yoo DJ. Profile of extended chemical stability and mechanical integrity and high hydroxide ion conductivity of poly(ether imide) based membranes for anion exchange membrane fuel cells. Int J Hydrogen Energy 2019;44:4281–92.
[22] Thieu LM, Zhu L, Korovich AG, Hickner MA, Madsen LA. Multiscale tortuous diffusion in anion and cation exchange membranes. Macromolecules 2019;52:24–35.
[23] Jiao K, Li X. Water transport in polymer electrolyte membrane fuel cells. Prog Energy Combust Sci 2011;37:221–91.
[24] Arges CG, Kambe Y, Dolejsi M, Wu G-P, Segal-Pertz T, Ren J, Cao C, Craig GSW, Nealey PF. Interconnected ionic domains enhance conductivity in microphase separated block copolymer electrolytes. J Mater Chem A 2017;5:5619–29.
[25] Marx D, Chandra A, Tuckerman ME. Aqueous basic solutions: hydroxide solvation, structural diffusion, and comparison to the hydrated proton. Chem Rev 2010;110:2174–216.
[26] H. Takaba, T. Hisabe, T. Shimizu,Md. K. Alam, Molecular modeling of OH- transport in poly(arylene ether sulfone ketone)s containing quaternized ammonio-substituted fluorenyl groups as anion exchange membranes.
[27] Chen C, Tse YS, Lindberg GE, Knight C, Voth GH. Hydroxide solvation and transport in anion exchange membranes. J Am Chem Soc 2016;138:991–1000.
[28] Hwang GS, Kaviany M, Gostick JT, Kientiz B, Weber AZ, Kim MH. Role of water states on water uptake and proton transport in Nafion using molecular simulations and bimodal network. Polymer 2011;52:2584–93.
[29] Zelovich T, Vogt-Maranto L, Hickner MA, Paddison SJ, Bae C, Dekel DR, Tuckerman ME. Hydroxide ion diffusion in anion-exchange membranes at low hydration: insights from ab initio molecular dynamics. Chem Mater 2019;31:5778–87.

Please cite this article as: Magnico P, Molecular dynamics study on water and hydroxide transfer mechanisms in PSU-g-alkyl-TMA membranes at low hydration: Effect of side chain length, International Journal of Hydrogen Energy, https://doi.org/10.1016/j.ijhydene.2021.07.081

[30] Zelovich T, Long Z, Hickner M, Paddison SJ, Bae C, Tuckerman ME. Ab initio molecular dynamics study of hydroxide diffusion mechanisms in nanoconfined structural mimics of anion exchange membranes. J Chem Phys C 2019;123:4638–53.
[31] Castañeda S, Ribadeneira R. Description of hydroxide ion structural diffusion in a quaternized SEBS anion exchange membrane using ab initio molecular dynamics. J Phys Chem C 2020;124:9834–51.
[32] Zadok I, Long H, Pivovar B, Roznowska A, Michalak A, Dekel DR, Srebnik S. Unexpected hydroxide ion structure and properties at low hydration. J Mol Liq 2020;313:113485.
[33] Zadok I, Dekel DR, Serbnik S. Effect of ammonium cations o the diffusivity and structure of the hydroxide ions in low hydration media. J Chem Phys C 2019;123:27355–37362.
[34] Shin DW, Guiver MD, Lee YM. Hydrocarbon-based polymer electrolyte membranes: importance of morphology on ion transport and membrane stability. Chem Rev 2017;117:4759–805.
[35] Lin CX, Zhuo YZ, Lai AN, Zhang QG, Zhu AM, Ye ML, Liu QL. Side-chain-type anion exchange membranes bearing pendent imidazolium-functionalized poly(phenylene oxide) for fuel cells. J Membr Sci 2016;513:206–16.
[36] Han J, Peng Y, Lin B, Zhu Y, Ren Z, Xiao L, Zhuang L. Hydrophobic side-chain attached polyarylether-based anion exchange membranes with enhanced alkaline stability. Appl Energy Mater 2019;2:8052–9.
[37] Li N, Yan T, Li Z, Thurn-Albrecht T, Binder WH. Comb-shaped polymers to enhance hydroxide transport in anion exchange membranes. Energy Environ Sci 2012;5:7888–92.
[38] Pan J, Han J, Zhu L, Hickner MA. Cationic side-chain attachment to poly(phenylene oxide) backbones for chemically stable and conductive anion exchange. Chem Mater 2017;29:5321–30.
[39] Chu L Liu X, Liao J, Huang Y, Li Y, Ge Z, Hickner MA, Li N. Tuning the properties of poly(2,6-dimethyl-1,4-phenylene oxide) anion exchange membranes and their performance in H2/O2 fuel cells. Energy Environ Sci 2018;11:435–46.
[40] Wang C, Xua C, Shena B, Zhaoa X, Lia J. Stable poly(arylene ether sulfone)s anion exchange imidazolium cations on pendant phenyl rings. Electrochem Acta 2016;190:1057–65.
[41] Han J, Gong S, Peng Z, Cheng X, Li Y, Peng H, Zhu Y, Ren Z, Xia L, Zhuang L. Comb-shaped anion exchange membranes: hydrophobic side chains grafted onto backbones or linked to cations? J Membr Sci 2021;626:119096.
[42] Wang Y, Qiao X, Liu M, Liu L, Li N. The effect of –NH– on quaternized polybenzimidazole anion exchange membranes for alkaline fuel cells. J Membr Sci 2021;626:119178.
[43] Dang H, Jannasch P. Exploring different cationic alkyl side chain designs for enhanced alkaline stability and hydroxide ion conductivity of anion-exchange membranes. Macromolecules 2015;48:5742–51.
[44] Al Munsur AZ, Hossain I, Nam SY, Chae JE, Kim T-H. Hydrophobic-hydrophilic comb-type quaternary ammonium-functionalized SEBS copolymers for high performance anion exchange membranes. J Membr Sci 2020;599:117829.
[45] Zhu L, Pan J, Christensen CM, Lin B, Hickner MA. Functionalization of poly(2,6-dimethyl-1,4-phenylene oxide) s with hindered fluorene side chains for anion exchange membranes. Macromolecules 2016;49:3300–9.
[46] Lee MT. Designing anion exchange membranes with enhanced hydroxide ion conductivity by mesoscale simulations. J Phys Chem C 2020;124:4470–82.
[47] Chen S, Wang H, Zhang J, Lu S, Xiang Y. Effect of side chain on the electrochemical performance of poly (ether ether ketone) based anion-exchange membrane: a molecular dynamics study. J Membr Sci 2020;605:118105.
[48] Wang C, Zhou Y, Xu C, Zhao X, Li J. Synthesis and properties of new side-chain-type poly(arylen ether sulfone)s containing tri-imidazole cations as anion-exchange membranes. Int J Hydrogen energy 2018;43:20739–49.
[49] Chen W, Yan X, Wu X, Huang S, Luo Y, Gong X, He G. Tri-quaternized poly (ether sulfone) anion exchange membranes with improved hydroxide conductivity. J Membr Sci 2016;514:613–21.
[50] Chen Y, Tao Y, Wang J, Yang S, Cheng S, Wei H, Ding Y. Comb-shaped guanidinium functionalized poly(ether sulfone)s for anion exchange membranes: effects of the spacer types and lengths. J Polym Sci, Part A: Polym Chem 2017;55:1313–21.
[51] Zhu L, Yu X, Hickner MA. Exploring backbone-cation alkyl spacers for multi-cation side chain anion exchange membranes. J Power Sources 2018;375:433–41.
[52] Case DA, Ben-Shalom IY, Brozell SR, Cerutti DS, Cheatham III TE, Cruzeiro VWD, Darden TA, Duke RE, Ghoreishi D, Giambasu G, Giese T, Gilson MK, Gohlke H, Goetz AW, Greene D, Harris R, Homeyer N, Huang Y, Izadi S, Kovalenko A, Krasny R, Kurtzman T, Lee TS, LeGrand S, Li P, Lin C, Liu J, Luchko T, Luo R, Man V, Mermelstein DJ, Merz KM, Miao Y, Monard G, Nguyen C, Nguyen H, Onufriev A, Pan F, Qi R, Roe DR, Roitberg A, Sagui C, Schott-Verdugo S, Shen J, Simmerling CL, Smith J, Swails J, Walker RC, Wang J, Wei H, Wilson L, Wolf RM, Wu X, Xiao L, Xiong Y, York DM, Kollman PA. Amber 2019. San Francisco: University of California; 2019.
[53] Martínez L, Andrade R, Birgin EG, Martínez JM. Packmol: a package for building initial configurations for molecular dynamics simulations. J Comput Chem 2009;30:2157–64.
[54] Martínez JM, Martínez L. Packing optimization for automated generation of complex system's initial configurations for molecular dynamics and docking. J Comput Chem 2003;24:819–25.
[55] Todorov I, Smith W, Trachenko K, Dove M. Dlpoly3: new dimensions in molecular dynamics simulations via massive parallelism. J Mater Chem 2006;16:1911.
[56] Wang J, Wolf RM, Caldwell JW, Kollman PA, Case DAJ. Development and testing of a general amber force field. J Comput Chem 2004;25:1157–74.
[57] Yong CW. Descriptions and implementations of DL_F notation: a natural chemical expression system of atom types for molecular simulations. J Chem Inf Model 2016;56:1405–9.
[58] Han KW, Ko KH, Abu-Hakmeh K, Bae C, Sohn YJ, Jang SS. Molecular dynamics simulation study on polysulfone-based anion exchange membrane in comparison with proton exchange membrane. J Chem Phys C 2014;118:12577–87.
[59] Abascal JLF, Vega C. A general purpose model for the condensed phases of water: TIP4P/2005. J Chem Phys 2005;123:234505.
[60] Dubey V, Maiti A, Daschakraborty S. Predicting the solvation structure and vehicular diffusion of hydroxide ion in an anion exchange membrane using nonreactive molecular dynamics simulation. Chem Phys Lett 2020;755:137802.
[61] Chen C, Tse Y-LS, Lindberg GE, Knight C, Voth GA. Hydroxide solvation and transport in anion exchange membranes. J Am Chem Soc 2016;138:991–1000.
[62] Zhang N, Huo J, Yang B, Ruan X, Zhang X, Bao J, Qi W, He G. Understanding of imidazolium group hydration, and polymer structure for hydroxide anion conduction in hydrated imidazolium-g-PP membrane by molecular dynamics simulations. Chem Eng Sci 2018;192:1167–76.
[63] Pandey TP, Maes AM, Sarode HN, Peters BD, Lavina S, Vezzu K, Yang Y, Poynton SD, Varcoe JR, Seifert S, Liberatore MW, Di Noto V, Herring AM. Phys Chem Chem Phys 2015;17:4367.

Please cite this article as: Magnico P, Molecular dynamics study on water and hydroxide transfer mechanisms in PSU-g-alkyl-TMA membranes at low hydration: Effect of side chain length, International Journal of Hydrogen Energy, https://doi.org/10.1016/j.ijhydene.2021.07.081

[64] Hammer R, Schönhoff M, Hansen MR. Comprehensive picture of water dynamics in nafion membranes at different levels of hydration. J Phys Chem B 2019;123:8313–24.
[65] Volkov VI, Chernyak AV, Gnezdilov OI, Skirda VD. Hydration, self-diffusion and ionic conductivity of Li+, Na+ and Cs+ cations in Nafion membrane studied by NMR. Solid State Ionics 2021;364:115627.
[66] Lingwood MD, Zhang Z, Kidd BE, McCreary KB, Houa J, Madsen LA. Unraveling the local energetics of transport in a polymer ion conductor. Chem Commun 2013;49:4283–5.
[67] Bizzarri A, Cannistraro S. Molecular dynamics of water at the protein-solvent interface. J Phys Chem B 2002;106:6617.
[68] Garcia AE, Stiller L. Computation of the mean residence time of water in the hydration shells of biomolecules. J Comput Chem 1993;14:1396–406.
[69] Rocchi Claudia, Bizzarri Anna Rita, Cannistraro Salvatore. Water dynamical anomalies evidenced by molecular-dynamics simulations at the solvent-protein interface. Phys Rev E 1998;57:3315–25.
[70] Gillois B, Goujon F, Fleury A, soldera A, Ghoufi A. Water nano-diffusion through the nafion fuel cell membrane. J Membr Sci 2020;602:117958.
[71] Hopkins P, Fortini A, Archer AJ, Schmidt M. The Van hove distribution function for Brownian hard spheres: dynamical test theory and computational simulations for bulk dynamics. J Phys Chem 2010;133:224505.
[72] Bernejo JS, Ugarte CM. Influence of water content on structure and mobility of polyvinyl alcohol: a molecular dynamics simulation. J Phys Chem 2008;129:154907.
[73] Linbach HJ, Ubink J. Structural and dynamics of maltooligomer-water solutions and glasses. Soft Matter 2008;4:1887.
[74] Tenuzzo L, Camisasca G, Gallo P. Protein-water and water-water long-time relaxations in protein hydration water upon cooling-A close look through density correlation functions. Molecules 2020;25:4570.
[75] De Marzio M, Camisasca G, Rovere M, Gallo P. Microscopic origin of the fragile to strong crossover in supercooled water: the role of activated processes. J Chem Phys 2017;146:084502.
[76] Attili A, Gallo P, Rovere M. Mode coupling behavior of a Lennard-Jones binary mixture: a comparison between bulk and confined phases. J Chem Phys 2005;123:174510.
[77] Schrøder TB. Hopping in disordered media: a model glass former and a hopping model. Ph.D. thesis. Roskilde University; 2018.
[78] Roberts CJ, Debenedetti Pablo G. Structure and dynamics in concentrated, amorphous carbohydrate-water systems by molecular dynamics simulation. J Phys Chem B 1999;103:7308–18.
[79] Huo J, Qi W, Zhu H, Yang B, He G, Bao J, Zhang X, Yan X, Gao L, Zhang N. Molecular dynamics simulation on the effect of water uptake on hydrogen bond network for OH^- conduction in imidazolium-g-PPO membrane. Int J Hydrogen energy 2019;44:3760–70.
[80] Luzar A, Chandler D. Effect of environment on hydrogen bond dynamics in liquid water. Phys Rev Lett 1996;76:928.
[81] Stoddard S. Identifying clusters in computer experiments on systems of particles. J Comput Phys 1978;27(2):291.

Please cite this article as: Magnico P, Molecular dynamics study on water and hydroxide transfer mechanisms in PSU-g-alkyl-TMA membranes at low hydration: Effect of side chain length, International Journal of Hydrogen Energy, https://doi.org/10.1016/j.ijhydene.2021.07.081